

AD-A142 313

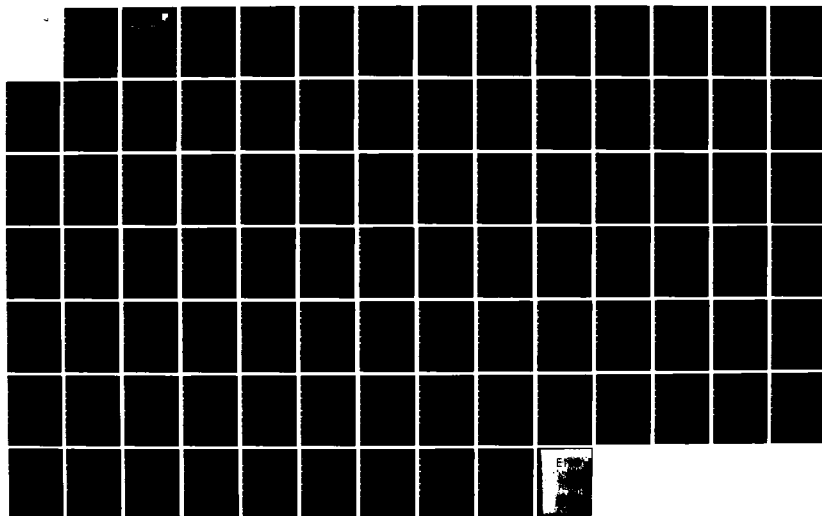
ANALYSIS AND PROGRAMMING FOR ELECTROMAGNETIC
APPLICATIONS(U) ARCON CORP WALTHAM MA E COHEN ET AL.
MAY 84 RADC-TR-84-95 F19628-81-C-0117

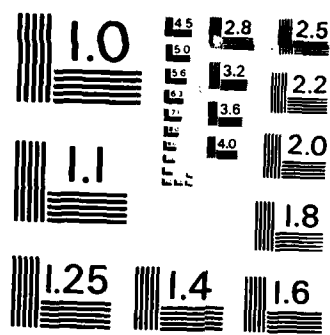
1/1

UNCLASSIFIED

F/G 12/1

NL





MICROCOPY RESOLUTION TEST CHART
NATIONAL BUREAU OF STANDARDS-1963-A

AD-A142 313

RADC-TR-84-95
Final Technical Report
May 1984



ANALYSIS AND PROGRAMMING FOR ELECTROMAGNETIC APPLICATIONS

ARCON Corporation

**Edward Cohen
Nataliya Itkin
Jewel Holst
Nancy Kerwin**

APPROVED FOR PUBLIC RELEASE; DISTRIBUTION UNLIMITED

NTC FILE COPY

**ROME AIR DEVELOPMENT CENTER
Air Force Systems Command
Griffiss Air Force Base, NY 13441**

JUN 21 1984

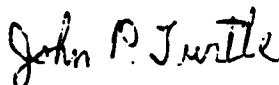
A

84 06 20 006

This report has been reviewed by the RADC Public Affairs Office (PA) and is releasable to the National Technical Information Service (NTIS). At NTIS it will be releasable to the general public, including foreign nations.

RADC-TR-84-95 has been reviewed and is approved for publication.

APPROVED:



JOHN P. TURTLÉ
Project Engineer

APPROVED:



ALLAN C. SCHELL
Chief, Electromagnetic Sciences Division

FOR THE COMMANDER:



JOHN A. RITZ
Acting Chief, Plans Office

If your address has changed or if you wish to be removed from the RADC mailing list, or if the addressee is no longer employed by your organization, please notify RADC (EEPS) Hanscom AFB MA 01731. This will assist us in maintaining a current mailing list.

Do not return copies of this report unless contractual obligations or notices on a specific document requires that it be returned.

UNCLASSIFIED

SECURITY CLASSIFICATION OF THIS PAGE

REPORT DOCUMENTATION PAGE				
1a. REPORT SECURITY CLASSIFICATION UNCLASSIFIED		1b. RESTRICTIVE MARKINGS N/A		
2a. SECURITY CLASSIFICATION AUTHORITY N/A		3. DISTRIBUTION/AVAILABILITY OF REPORT Approved for public release; Distribution unlimited		
2b. DECLASSIFICATION/DOWNGRADING SCHEDULE N/A				
4. PERFORMING ORGANIZATION REPORT NUMBER(S) N/A		5. MONITORING ORGANIZATION REPORT NUMBER(S) RADC-TR-84-95		
6a. NAME OF PERFORMING ORGANIZATION ARCON Corporation	6b. OFFICE SYMBOL (If applicable)	7a. NAME OF MONITORING ORGANIZATION Rome Air Development Center (EEPS)		
6c. ADDRESS (City, State and ZIP Code) 260 Bear Hill Road Waltham MA 02154		7b. ADDRESS (City, State and ZIP Code) Hanscom AFB MA 01731		
8a. NAME OF FUNDING/SPONSORING ORGANIZATION Rome Air Development Center	8b. OFFICE SYMBOL (If applicable) EEPS	9. PROCUREMENT INSTRUMENT IDENTIFICATION NUMBER F19628-81-C-0117		
8c. ADDRESS (City, State and ZIP Code) Hanscom AFB MA 01731		10. SOURCE OF FUNDING NOS.		
		PROGRAM ELEMENT NO. 62702F	PROJECT NO. 4600	TASK NO. 16 WORK UNIT NO. 57
11. TITLE (Include Security Classification) ANALYSIS AND PROGRAMMING FOR ELECTROMAGNETIC APPLICATIONS				
12. PERSONAL AUTHOR(S) Edward Cohen, Nataliya Itkin, Jewel Holst and Nancy Kerwin				
13a. TYPE OF REPORT Final	13b. TIME COVERED FROM Jul81 TO Dec83	14. DATE OF REPORT (Yr., Mo., Day) May 1984	15. PAGE COUNT 94	
16. SUPPLEMENTARY NOTATION				
17. COSATI CODES		18. SUBJECT TERMS (Continue on reverse if necessary and identify by block number)		
FIELD	GROUP	SUB. GR.		
17	02	Electromagnetic Sciences VLF Propagation MSW Transducers LF Propagation Meteor Scatter OTH Radars		
19. ABSTRACT (Continue on reverse if necessary and identify by block number) During the last 30 months, our technical work consisted of providing RADC scientists with mathematical and programming support in the following areas: magnetostatic wave transducer analysis; antenna analysis and design studies; conversion, implementation, and execution of ionospheric propagation programs; radar data analysis; electromagnetic scattering from rough terrains, etc. This work resulted in the development of mathematical models and computer programs. When desired, we functioned in a collaborative manner to assist with the physical formulation problems of interest.				
20. DISTRIBUTION/AVAILABILITY OF ABSTRACT UNCLASSIFIED/UNLIMITED <input checked="" type="checkbox"/> SAME AS RPT. <input type="checkbox"/> OTIC USERS <input type="checkbox"/>		21. ABSTRACT SECURITY CLASSIFICATION UNCLASSIFIED		
22a. NAME OF RESPONSIBLE INDIVIDUAL John P. Turtle		22b. TELEPHONE NUMBER (Include Area Code) (617) 861-4239	22c. OFFICE SYMBOL EEPS	

DD FORM 1473, 83 APR

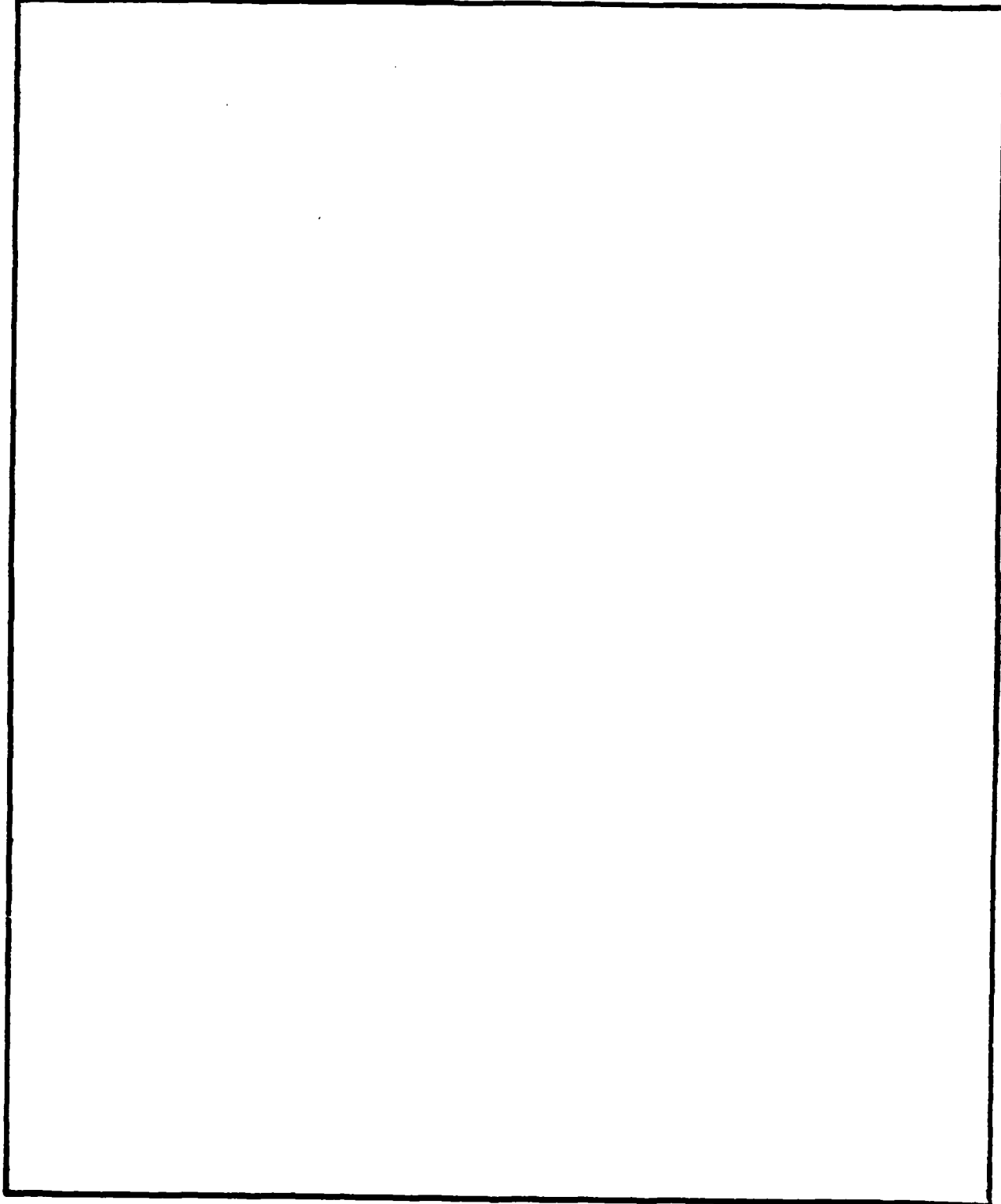
EDITION OF 1 JAN 73 IS OBSOLETE.

UNCLASSIFIED

SECURITY CLASSIFICATION OF THIS PAGE

UNCLASSIFIED

SECURITY CLASSIFICATION OF THIS PAGE



UNCLASSIFIED

SECURITY CLASSIFICATION OF THIS PAGE

TABLE OF CONTENTS

<u>Section</u>	<u>Page</u>
1. INTRODUCTION	1
2. MSSW Transducer Analysis	2
2.1 Introduction	2
2.2 Transducer Green's Function Analysis - Introduction	3
2.3 Derivation of Two-Dimensional Field Equations	3
2.4 Extended MSW Analysis	12
2.5 Evaluation of $\alpha \pm$	20
2.6 Integration Over the Interval $(0, 2U_M)$	21
2.7 Integration Over the Semi-infinite Interval $(2U_M, \infty)$	23
2.8 Half-Period Integration	25
2.9 Results and Discussion	28
3. MODESEARCH and FASTMC Program Conversions and Implementations	52
4. OTH Radar Data Analysis	60
4.1 Introduction	60
4.2 Program POWERLEVEL	61
4.3 Program BINSORT	61
4.4 Program SPEEDSORT	62
4.5 Program SPREADSORT	64
5. Meteor Scatter Model	69
6. Direct and Multipath Communications Data Analysis	74
6.1 Introduction	74
6.2 Data Tape Content and Task Orientation	74
6.3 Correlation Analysis	75
6.4 Fast Correlation	76



PREFACE

The analysis, computer programs and results discussed herein are the result of research and programming performed for

Rome Air Development Center
Electromagnetic Sciences Division
L. G. Hanscom Air Force Base, Massachusetts 01731

1. INTRODUCTION

During the last 30 months, our technical work consisted of providing RADC scientists with mathematical and programming support in the following areas: magnetostatic wave transducer analysis; antenna analysis and design studies; conversion, implementation, and execution of ionospheric propagation programs; radar data analysis; electromagnetic scattering from rough terrains, etc. This work resulted in the development of mathematical models and computer programs. When desired, we functioned in a collaborative manner to assist with the physical formulation of problems of interest. This report presents a representative selection of our efforts.

2. MSSW Transducer Analysis

2.1 Introduction

The development of mathematical models for describing the response features of magnetostatic surface wave (MSSW) devices has been of considerable interest to the Air Force. Despite previous successes at predicting the behavior of transducers lifted off a YIG substrate, the models have proved to be inadequate for describing, with sufficient accuracy, the response of multi-element transducer arrays very near or on a magnetically biased YIG slab. Strong coupling effects appear to become important in these situations. Our efforts during this contract were aimed at developing models for predicting transducer characteristics under strong coupling conditions.

In keeping with the initiator's objectives, a sequence of investigations was undertaken to develop current density models for multi-element arrays on or near a YIG slab. The first study entailed determining current density over mutually coupled conducting strips near a ground plane; no YIG material being present to influence the distributions. The Fourier transforms of the resulting current profiles were incorporated into the Weinberg programs [Ref. 1] for predicting, among other things, transducer insertion loss. The details of the analysis as well as the results have been previously described in Ref. 2. The current distributions did not lead to some of the insertion loss features that appear experimentally. Even when replacing the ground plane with a highly permeable ($\mu \rightarrow \infty$) magnetic half-space, the insertion loss predictions did not improve. From the investigations it was concluded that mutual coupling among the strips and ground plane (or magnetic half-space) does not by itself appear to be the key mechanism for causing some of the dominant response features observed in the surface wave passband.

The results noted above led us to several Green's function analyses. By posing (and solving) a sufficiently well modeled boundary-value problem describing the field about a time-harmonic line current source near a YIG slab, in principle one can obtain the current density on a planar array of infinitely long, thin, perfectly conducting strips on or near a ferrite slab. The current density on each strip can be thought of as arising from a continuum of line currents. Obtaining the Green's function, or total influence function, of the magnetically biased slab on the vector potential field about the line source became the focus of most of the work to be reported in this section.

2.2 Transducer Green's Function Analysis - Introduction

The geometry of MSSW transducers is often such that source and field quantities can be assumed to vary much more strongly with x and y than z . A two-dimensional field theory approximation was, therefore, invoked for determining the Green's function of an array between a ground plane and YIG slab. (See Fig. 2.1.) The strips were also assumed to be sufficiently close to the YIG and each other so that

$$0 < k_1 R \ll 1 ; \quad (1)$$

k_1 is the electromagnetic wave number in the medium (GGG) above and below the YIG, and R is the distance from any line current element on a strip to any field point of interest. Field points on nearby strips or on the nearest regions of the YIG slab surfaces are most important regarding mutual coupling and generation of MSSWs. It was assumed, therefore, that all field points required for a current density analysis were located in the quasi-static zone of the rf field of the line currents. At frequencies between 2.5 - 3.5 Ghz, this assumption appears to be reasonable for typical MSSW arrays composed of a few strip elements.

2.3 Derivation of Two-Dimensional Field Equations

The two-dimensional approximation discussed above leads to a considerable simplification of the analysis. Maxwell's equations must be satisfied

in the 3 regions as must the boundary conditions at the surfaces $y = (D+d)$, $y = 0$, and $y = -h$. With

$$\begin{aligned}\underline{B}^{(1)} &= \mu \cdot \underline{H}^{(1)} \equiv \nabla \times \underline{A}^{(1)} ; \\ \underline{B}^{(2)} &= \mu \cdot \underline{\mu} \underline{H}^{(2)} \equiv \nabla \times \underline{A}^{(2)} ; \\ \underline{B}^{(3)} &= \mu \cdot \underline{H}^{(3)} \equiv \nabla \times \underline{A}^{(3)} ;\end{aligned}\tag{2}$$

$$\begin{aligned}\nabla \cdot \underline{B}^{(1)} &= \nabla \cdot \underline{B}^{(2)} = \nabla \cdot \underline{B}^{(3)} = 0 ; \\ \nabla \cdot \underline{D}^{(1)} &= \nabla \cdot \underline{D}^{(2)} = \nabla \cdot \underline{D}^{(3)} = 0 ;\end{aligned}\tag{3}$$

$$\underline{\mu} = \begin{pmatrix} \mu_{11} & i\mu_{12} \\ -i\mu_{12} & \mu_{22} \end{pmatrix}; \quad \underline{\mu}^{-1} = \begin{pmatrix} \bar{b} & -\bar{e} \\ \bar{e} & \bar{c} \end{pmatrix};\tag{4}$$

(based on the linearized magnetization equation)

where

$$\bar{b} = \bar{c} = \frac{\mu_{11}}{\mu_{11}^2 - \mu_{12}^2},\tag{5}$$

$$\underline{\mu}^{-1} \underline{\mu} = \underline{I},\tag{6}$$

and

$$\bar{e} = \frac{i\mu_{12}}{\mu_{11}^2 - \mu_{12}^2} \quad (7)$$

for the surface wave case in which $\mu_{11} = \mu_{22}$. Maxwell's equations in the 3 regions take the following form:

$$\left\{ \begin{array}{l} \nabla \times (\nabla \times \underline{A}^{(1)}) = \mu_0 \underline{J} + \mu_0 \frac{\partial \underline{D}^{(1)}}{\partial t} ; \end{array} \right. \quad (8)$$

$$\left\{ \begin{array}{l} \nabla \times \underline{E}^{(1)} = - \frac{\partial}{\partial t} (\nabla \times \underline{A}^{(1)}) ; \end{array} \right. \quad (9)$$

$$\nabla \times (\underline{\mu}^{-1} \nabla \times \underline{A}^{(2)}) = \mu_0 \frac{\partial \underline{D}^{(2)}}{\partial t} ; \quad (10)$$

$$\nabla \times \underline{E}^{(2)} = - \frac{\partial}{\partial t} (\nabla \times \underline{A}^{(2)}) ; \quad (11)$$

$$\nabla \times (\nabla \times \underline{A}^{(3)}) = \mu_0 \frac{\partial \underline{D}^{(3)}}{\partial t} ; \quad (12)$$

$$\nabla \times \underline{E}^{(3)} = - \frac{\partial}{\partial t} (\nabla \times \underline{A}^{(3)}) . \quad (13)$$

(9) yields

$$\underline{E}^{(1)} = - \frac{\partial \underline{A}^{(1)}}{\partial t} - \nabla \phi^{(1)} \quad (14)$$

and (8) becomes

$$\nabla(\nabla \cdot \underline{A}^{(1)}) - \nabla^2 \underline{A}^{(1)} = \mu_0 \underline{J} + \epsilon_1 \mu_0 \frac{\partial \underline{E}^{(1)}}{\partial t}. \quad (15)$$

Inserting the expression for $\underline{E}^{(1)}$ into the above gives

$$\nabla(\nabla \cdot \underline{A}^{(1)}) - \nabla^2 \underline{A}^{(1)} = \mu_0 \underline{J} - \epsilon_1 \mu_0 \left[\frac{\partial^2 \underline{A}^{(1)}}{\partial t^2} + \nabla \left(\frac{\partial \Phi^{(1)}}{\partial t} \right) \right]. \quad (16)$$

Applying the Lorentz condition:

$$\nabla \cdot \underline{A}^{(1)} + \epsilon_1 \mu_0 \frac{\partial \Phi^{(1)}}{\partial t} = 0. \quad (17)$$

leaves

$$\nabla^2 \underline{A}^{(1)} - \epsilon_1 \mu_0 \frac{\partial^2 \underline{A}^{(1)}}{\partial t^2} = -\mu_0 \underline{J}. \quad (18)$$

Similarly, for region (3):

$$\nabla^2 \underline{A}^{(3)} - \epsilon_3 \mu_0 \frac{\partial^2 \underline{A}^{(3)}}{\partial t^2} = 0 \quad (19)$$

when

$$\nabla \cdot \underline{A}^{(3)} + \epsilon_3 \mu_0 \frac{\partial \Phi^{(3)}}{\partial t} = 0. \quad (20)$$

For region (2), since

$$\nabla \times (\underline{\mu}^{-1} \nabla \times \underline{A}^{(2)}) = \underline{\mu}^{-1} \nabla (\nabla \cdot \underline{A}^{(2)}) - (\nabla \cdot \underline{\mu}^{-1} \nabla) \underline{A}^{(2)} \quad (21)$$

we get

$$\underline{\mu}^{-1} \nabla (\nabla \cdot \underline{A}^{(2)}) - (\nabla \cdot \underline{\mu}^{-1} \nabla) \underline{A}^{(2)} = \mu_0 \epsilon_2 \frac{\partial}{\partial t} \left[-\frac{\partial \underline{A}^{(2)}}{\partial t} - \nabla \phi^{(2)} \right]. \quad (22)$$

The desired gauge requires the condition

$$\underline{\mu}^{-1} \nabla (\nabla \cdot \underline{A}^{(2)}) + \mu_0 \epsilon_2 \frac{\partial}{\partial t} (\nabla \phi^{(2)}) = 0, \quad (23)$$

leaving

$$- (\nabla \cdot \underline{\mu}^{-1} \nabla) \underline{A}^{(2)} + \mu_0 \epsilon_2 \frac{\partial^2 \underline{A}^{(2)}}{\partial t^2} = 0. \quad (24)$$

Since \underline{J} and \underline{H}_0 are aligned parallel to the z-axis,

$$\underline{A} = A_z \hat{z} \quad (25)$$

and

$$\underline{J} = J_z \hat{z}. \quad (26)$$

Assuming

$$A_z = A e^{-i\omega t} \quad (27)$$

and

$$J_z = J e^{-i\omega t} \quad (28)$$

the exact, linearized wave equations governing the vector potential fields in the 3 regions reduce to

$$\nabla^2 A^{(1)} + \mu_0 \epsilon_1 \omega^2 A^{(1)} = -\mu_0 J; \quad (29)$$

$$\nabla \cdot (\underline{\mu}^{-1} \nabla) A^{(2)} + \mu_0 \epsilon_2 \omega^2 A^{(2)} = 0; \quad (30)$$

$$\nabla^2 A^{(3)} + \mu_0 \epsilon_3 \omega^2 A^{(3)} = 0. \quad (31)$$

Expanding the wave equations in Cartesian components leads to the following equations for a line current at $x = 0, y = d$:

$$A_{xx}^{(0)} + A_{yy}^{(0)} + \mu_0 \epsilon_1 \omega^2 A^{(0)} = -\mu_0 I \delta(x) \delta(y-d) ; \quad (32)$$

$$A_{xx}^{(2)} + A_{yy}^{(2)} + \frac{\mu_0 \epsilon_2 \omega^2}{b} A^{(2)} = 0 ; \quad (33)$$

$$A_{xx}^{(3)} + A_{yy}^{(3)} + \mu_0 \epsilon_3 \omega^2 A^{(3)} = 0 . \quad (34)$$

As noted earlier, the current on any strip can be expressed as a continuous density of line currents. It follows that the total vector potential for a strip can be regarded as a superposition of the vector potentials caused by a weighted density of line currents. The vector potential for a single line current, i.e., the Green's function of the system, can be found by solving the system of wave equations subject to the boundary conditions. The Green's function, G , is proportional to the vector potential and contains all of the influences that affect the current densities. The boundary conditions that A (or G) must satisfy will now be derived.

Since

$$\underline{\nabla} \times \underline{A} = \hat{z} A_y - \hat{y} A_x , \quad (35)$$

it follows that

$$\underline{H}^{(n)} = \begin{pmatrix} H_1^{(n)} \\ H_2^{(n)} \end{pmatrix} = \frac{1}{\mu_0} \begin{pmatrix} A_y^{(n)} \\ -A_x^{(n)} \end{pmatrix} ; \quad (36)$$

with $m = 1, 3$ for regions 1 and 3. For the slab region

$$\underline{H}^{(3)} = \frac{1}{\mu_0} \underline{\mu}^{-1} \begin{pmatrix} A_y^{(3)} \\ -A_x^{(3)} \end{pmatrix} \quad (37)$$

$$= \frac{1}{\mu_0} \begin{pmatrix} \bar{b} & -\bar{e} \\ \bar{e} & \bar{b} \end{pmatrix} \begin{pmatrix} A_y^{(3)} \\ -A_x^{(3)} \end{pmatrix} = \frac{1}{\mu_0} \begin{pmatrix} \bar{b} A_y^{(3)} + \bar{e} A_x^{(3)} \\ \bar{e} A_y^{(3)} - \bar{b} A_x^{(3)} \end{pmatrix}. \quad (38)$$

The boundary conditions at the ground plane and YIG surfaces may be summarized as follows:

$$\underline{B}_n^{(1)} = 0 \quad \text{at} \quad y = D + d; \quad (39)$$

$$\underline{B}_n^{(1)} = \underline{B}_n^{(2)} \quad \text{and} \quad (40)$$

$$\underline{H}_t^{(1)} = \underline{H}_t^{(2)} \quad \text{at} \quad y = 0; \quad (41)$$

$$\underline{B}_n^{(3)} = \underline{B}_n^{(2)} \quad \text{and} \quad (42)$$

$$\underline{H}_t^{(3)} = \underline{H}_t^{(2)} \quad \text{at} \quad y = -h. \quad (43)$$

Using the relationships among \underline{B} , \underline{H} and \underline{A} , the boundary conditions may be written in terms of the $\underline{A}^{(m)}$ alone:

$$\text{at} \quad y = D + d, \quad A_x^{(1)} = 0; \quad (44)$$

$$\text{at} \quad y = 0 \quad A_x^{(1)} = A_x^{(2)} \quad (45)$$

$$\text{and} \quad A_y^{(1)} = \bar{b} A_y^{(2)} + \bar{e} A_x^{(2)} ; \quad (46)$$

$$\text{at } y = -h \quad A_x^{(1)} = A_x^{(2)} \quad (47)$$

$$\text{and} \quad A_y^{(3)} = \bar{b} A_y^{(2)} + \bar{e} A_x^{(2)} . \quad (48)$$

The propagation constants for the 3 regions are given by equations (29-31):

$$k_1^2 = \mu_0 \epsilon_1 \omega^2 ; \quad (49)$$

$$k_2^2 = \mu_0 \epsilon_2 \omega^2 / \bar{b} \quad (50)$$

$$\text{and} \quad k_3^2 = \mu_0 \epsilon_3 \omega^2 . \quad (51)$$

At frequencies within the surface wave passband, k_2^2 is negative and is denoted by $k_2^2 \equiv -k_s^2$. In the quasi-magnetostatic approximation the wave equations are approximated by

$$A_{xx}^{(1)} + A_{yy}^{(1)} \approx -\mu_0 I \delta(x) \delta(y-d) ; \quad (52)$$

$$A_{xx}^{(2)} + A_{yy}^{(2)} \approx 0 ; \quad (53)$$

$$A_{xx}^{(3)} + A_{yy}^{(3)} \approx 0 . \quad (54)$$

This is equivalent to neglecting the displacement current, i.e., radiation term, in the curl \underline{H} equation for each region.

2.4 Extended MSW Analysis

We found that it was important to retain the term involving $(k_s^2 A^{(2)})$ for the YIG region. That term has very little effect on the MSW's wave-number over most of the surface wave band; however, it introduces a long period surface wave in addition to the MSSW and other important effects. The extended quasi-magnetostatic surface wave equations may thus be summarized as follows:

$$A_{xx}^{(1)} + A_{yy}^{(1)} \approx -\mu_0 I \delta(x) \delta(y-d); \quad (55)$$

$$A_{xx}^{(2)} + A_{yy}^{(2)} - k_s^2 A^{(2)} = 0; \quad (56)$$

$$A_{xx}^{(3)} + A_{yy}^{(3)} \approx 0. \quad (57)$$

Upon solution, \underline{B} and \underline{E} follow from (2,14) and similar formulas for the other regions: since $\nabla\phi = \frac{\partial\phi}{\partial z} \hat{z} = 0$ in a pure, two-dimensional formulation where there is no z-variation, ϕ is not required in the expression for \underline{E} .

The solutions for each region that satisfy the extended MSW equations may be written as:

$$a^{(1)} \equiv \frac{A^{(1)}}{(\mu_0 I / 4\pi)} \approx \ln [x^2 + (y-d)^2] + \int_{-\infty}^{\infty} dk e^{ikx} [B_1 e^{-|k|y} + B_2 e^{|k|y}]; \quad (58)$$

$$a^{(2)} \equiv \frac{A^{(2)}}{(\mu_0 I / 4\pi)} = \int_{-\infty}^{\infty} dk e^{ikx} [C_1 e^{y\sqrt{k^2 + k_s^2}} + C_2 e^{-y\sqrt{k^2 + k_s^2}}]; \quad (59)$$

$$a^{(5)} \equiv \frac{A^{(5)}}{(\mu_0 I / 4\pi)} \approx \int_{-\infty}^{\infty} dk e^{ikx} D_1 e^{(y+h)/k} \quad (60)$$

For region ①, the direct field due to the line source alone has been separated out of the general solution, i.e., the unbounded Green's function term

$$\begin{aligned} & \frac{\mu_0 I}{2\pi} \ln [x^2 + (y-d)^2]^{\frac{1}{2}} \\ &= \frac{(\mu_0 I)}{4\pi} \ln [x^2 + (y-d)^2] \end{aligned} \quad (61)$$

All potentials are then made dimensionless by dividing out the factor $(\mu_0 I / 4\pi)$ for convenience. The normalized vector potential or Green's function for each region is to be found for a line source at $(0, d)$. The $|k|$ - factors in the expressions for $A^{(1)}$ and $A^{(3)}$ are rigorously correct only for pure static fields. The implications for a quasistatic analysis become apparent shortly. Also, while the Green's function for a quasistatic line source varies as

$$\begin{aligned} & \ln k_1 R(x, y-d) \\ &= \ln k_1 + \ln R(x, y-d), \end{aligned} \quad (62)$$

the term $\ln k_1$ may be dropped now (or later) because all the boundary conditions involve spatial derivatives in x and y . The vector potentials are thus arbitrary to within a constant level of potential. B_1 , B_2 , C_1 , C_2 , and D_1 are all, as yet, unknown functions of k . Inserting the solutions into the boundary conditions, and solving for the unknown spectral amplitudes, we arrived at the following expression for $a^{(1)}$ in the

important limiting case for $D \rightarrow \infty$:

$$a^{\odot} = \ln [x^2 + (y-d)^2] + \int_{-\infty}^{\infty} dk \frac{e^{\alpha(k)} g(k)}{\bar{D}(k)} + \bar{b}^2 k_s^2 \int_{-\infty}^{\infty} dk \frac{e^{\alpha(k)}}{|k| \bar{D}(k)}, \quad (63)$$

where

$$\alpha(k) = i k x - |k| (y+d), \quad (64)$$

$$g(k) = |k| \left[\bar{b}^2 - (1 - i \bar{e} \sin(k)) \right], \quad (65)$$

$$\equiv |k| g_{\pm}$$

and

$$\bar{D}(k) = [|k|^2 + k^2 (\bar{e}^2 + \bar{b}^2) + k_s^2 \bar{b}^2] + 2 \bar{b} |k| \sqrt{k^2 + k_s^2} \coth (k \sqrt{k^2 + k_s^2}). \quad (66)$$

One of the findings of the extended MSW formulation was that $\bar{D}(k)$ possesses zeros at

$$k = \pm k_0 \quad \text{and} \quad (67)$$

$$k = \pm k_{MSW}. \quad (68)$$

The poles of the integrands at $\pm k_0$ are very near the origin and lead to very long period surface waves. Earlier MSSW analyses do not reveal such poles because of their simpler characteristic equation; namely,

$$\lim_{k_z \rightarrow 0} \bar{\Phi}(k) = 0 = (1 + \bar{e}^2 + \bar{b}^2) + 2\bar{b} \coth(|k|h). \quad (69)$$

The poles near the origin are located to an excellent approximation at

$$k_0 \approx \pm \frac{1}{2} |\bar{b}| k_z^2 h. \quad (70)$$

Gerson and Nadan [Ref. 3] report other "dynamic" modes in their plane wave analysis involving the exact set of Maxwell's equations. A comparison between their results and ours in this regard is by necessity incomplete as of this writing.

The problem that remains for determining the Green's function is the evaluation of the two Fourier integrals shown in (63). They contain the effect of the YIG on the total vector potential and are denoted by

$$a_{YIG}^{(1)} = \int_{-\infty}^{\infty} dk e^{\alpha(k)} \frac{|k| g(k)}{\bar{\Phi}(k)} + \bar{\Phi}(0) \int_{-\infty}^{\infty} dk \frac{e^{\alpha(k)}}{|k| \bar{\Phi}(k)}. \quad (71)$$

Since $\bar{b}^2 k_z^2 = \bar{\Phi}(0)$, and taking into account that with an $\exp(-i\omega t)$ variation fields propagating in the $\pm x$ directions correspond to $\exp(\pm i k x)$,

we can express $a_{YIG}^{(1)}$ as follows:

$$\begin{aligned}
 a_{YIG}^{(1)} &= \int_0^{\infty} dk e^{\pm i k x} e^{-|k|(y+d)} \frac{k g_{\pm}}{\bar{D}(k)} \\
 &\quad + \int_0^{\infty} dk e^{\pm i k x} e^{-|k|(y+d)} \frac{\bar{D}(0)}{|k| \bar{D}(k)} \\
 &\equiv a_{\pm}
 \end{aligned} \tag{72}$$

a_{+} is to be evaluated for a field point at $+x$ and source point at $x=0$; a_{-} for the field point at $-x$ and source at $x=0$. For a low loss YIG slab, $\bar{D}(k)$ possesses zeros at $k \approx \pm k_0, \pm k_{MSSW}$, none of which are at the origin; all of which are very near the real k axis.

The 2nd integral in particular requires special treatment as will now be discussed. Note that it is equal to

$$\begin{aligned}
 &\int_0^{\infty} dk \frac{e^{\pm i k x}}{|k|} e^{-k(y+d)} \left[\frac{\bar{D}(0)}{\bar{D}(k)} - 1 \right] \\
 &\quad + \lim_{\epsilon \rightarrow 0} \int_{\epsilon}^{\infty} dk \frac{e^{\pm i k x}}{|k|} e^{-k(y+d)}.
 \end{aligned} \tag{73}$$

The 1st part is non-singular at $k=0$, and the 2nd may be related to the Exponential integral of complex argument. Let $k = \epsilon v$. It follows that

$$\lim_{\epsilon \rightarrow 0} \int_{\epsilon}^{\infty} dk \frac{e^{-k[y+d \mp i|x|]}}{k} \quad (74)$$

$$= \lim_{\epsilon \rightarrow 0} \int_1^{\infty} dv \frac{e^{-\epsilon[y+d - i|x|]v}}{v} \quad (75)$$

$$= \lim_{\epsilon \rightarrow 0} E_1[\epsilon(y+d - i|x|)]. \quad (76)$$

See Ref. 4 . For $\epsilon \rightarrow 0$,

$$E_1(z) \rightarrow -\gamma_E - \ln z + \dots \quad (77)$$

$$= -\gamma_E - \ln \epsilon(y+d - i|x|) + \dots \quad (78)$$

$$= \underbrace{-\gamma_E - \ln \epsilon}_{\text{spatially uniform terms}} - \ln \left(\sqrt{x^2 + (y+d)^2} e^{-i \tan^{-1} \left(\frac{|x|}{y+d} \right)} \right) + \dots \quad (79)$$

$$\rightarrow -\frac{1}{2} \ln [x^2 + (y+d)^2] + i \tan^{-1} \left(\frac{|x|}{y+d} \right) + \dots, \quad (80)$$

with γ_E = Euler's constant. Since spatially uniform terms, however large or small, contribute nothing of physical consequence to the vector potential, such terms may be discarded. Collecting physically meaningful terms leads to

$$\begin{aligned}
 A_{\pm} = & \int_0^{\infty} dk \frac{e^{-k[\gamma+d-i|x|]}}{k \bar{D}(k)} \\
 & + \int_0^{\infty} dk \frac{e^{-k[\gamma+d-i|x|]}}{k} \left[\frac{\bar{D}(\infty)}{\bar{D}(k)} - 1 \right] \\
 & - \frac{1}{2} \ln [x^2 + (\gamma+d)^2] + i \tan^{-1} \left(\frac{|x|}{\gamma+d} \right).
 \end{aligned} \tag{81}$$

For an analysis based on the exact equations (32-34) and $\epsilon_1 = \epsilon_3$, $|k|$ would be replaced by $\sqrt{k^2 - k_1^2}$. In the quasistatic approximation, one must think in terms of propagating fields with

$$\sqrt{k^2 - k_1^2} \rightarrow \lim_{k_1 \rightarrow 0} \sqrt{k^2 - k_1^2} = \lim_{\epsilon \rightarrow 0} \sqrt{k^2 - \epsilon^2} \rightarrow |k| + \dots, \tag{82}$$

hence the need for the limiting process in (73). For a pure static analysis, $k_1 = 0$ identically. No resolution into separate propagating fields in either

the +x or -x direction is to be made in this case. One encounters, rigorously, an integral of the form

$$\int_{-\infty}^{\infty} dk \frac{e^{ikx} e^{-|k|(y+d)}}{|k|} \quad (83)$$

that holds for all x and y and whose "value", in the sense of generalized functions, is given by

$$-\ln [x^2 + (y+d)^2] + \text{Const.} \quad (84)$$

See Lighthill [Ref. 5]. Assembling terms and making the following change of variables, the integrals comprising $a_{YIG}^{(1)}$ are then ready for evaluation. Let

$$k_M = k_{MSSW}, \quad (85)$$

$$U = kh, \quad \text{and} \quad (86)$$

$$\gamma = [y+d - i|x|]/h \quad (87)$$

$$= k_M [y+d - i|x|]/(k_M h) \quad (88)$$

$$\equiv [\bar{\beta} - i|\bar{x}|]/U_M. \quad (89)$$

The total vector potential becomes

$$a^{(1)} = \ln [x^2 + (y-d)^2] + a_{\pm} \quad (90)$$

where

$$a_{\pm} = \int_0^{\infty} dU e^{-\gamma U} \left\{ \frac{U g_{\pm}}{\bar{B}(U)} + \frac{\frac{\bar{B}(0)}{\bar{B}(U)} - 1}{U} \right\} - \frac{1}{2} \ln [x^2 + (y+d)^2] + i \tan^{-1} \left(\frac{|\bar{x}|}{\bar{\beta}} \right), \quad (91)$$

with

$$\bar{\theta}(u) = \bar{\theta}(0) + u^2(1 + \bar{e} + \bar{b}) + 2\bar{b}u\sqrt{u^2 + u_s^2} \coth(\sqrt{u^2 + u_s^2}), \quad (92)$$

and

$$\bar{\theta}(0) = \bar{b}^2 u_s^2 = \bar{b}^2 (k_s h)^2. \quad (93)$$

2.5 Evaluation of a_{\pm}

A direct numerical evaluation of a_{\pm} was accomplished using the methods of Real Axis Integration [Refs. 6,7]. For a nearly lossless medium there are 2 poles along the path of integration which is infinitesimally near the real U-axis. The pole locations are at

$$U = U_0 \approx \frac{1}{2} |\bar{b}| u_s^2 \quad (94)$$

and

$$U = U_M = k_M h, \quad (95)$$

where $U = kh$, $U_0 = k_0 h$, and $U_s = k_s h$. To evaluate the one-sided Fourier integrals in the sense of Cauchy Principal-Value, the semi-infinite range $(0, \infty)$ is partitioned into the ranges $(0, 2U_M)$ and $(2U_M, \infty)$. The two poles are located in the first interval and satisfy the relationship

$$0 < U_0 \ll U_M < 2U_M. \quad (96)$$

The problem reduced to the evaluation of

$$\int_0^{\infty} du e^{-\gamma u} f(u) = \int_0^{\infty} du e^{-\gamma u} \left\{ \frac{U g_{\pm}}{\bar{\theta}(u)} + \frac{\frac{\bar{\theta}(u)}{\bar{\theta}(0)} - 1}{u} \right\} \quad (97)$$

$$= \int_0^{2U_M} du e^{-\gamma u} f(u) + \int_{2U_M}^{\infty} du e^{-\gamma u} f(u). \quad (98)$$

2.6 Integration Over the Interval $(0, 2U_M)$

The singularities at U_0 and U_M were analytically removed from the integrand, and their contributions added back into the final answer separately, viz.,

$$\begin{aligned} \int_0^{2U_M} du e^{-\gamma u} f(u) &= \int_0^{2U_M} du e^{-\gamma u} \left[f(u) - \frac{C_0}{u-u_0} - \frac{C_M}{u-u_M} \right] \\ &+ \int_0^{2U_M} du e^{-\gamma u} \left[\frac{C_0}{u-u_0} + \frac{C_M}{u-u_M} \right]. \end{aligned} \quad (99)$$

The 2nd integral, although singular, is easily evaluated; the 1st integral is now non-singular. To determine C_0 and C_M , express $f(u)$ as

$$f(u) = \frac{n(u)}{\bar{\theta}(u)}, \quad (100)$$

where $n(u)$ is a numerator function.

Then, as $u \rightarrow u_0$

$$f(u) = \frac{C_0}{u-u_0} + \dots \quad (101)$$

or

$$C_0 = \lim_{u \rightarrow u_0} (u-u_0) f(u). \quad (102)$$

It follows that

$$C_0 = \lim_{v \rightarrow v_0} (v - v_0) \frac{n(v)}{\bar{\theta}(v)} \quad (103)$$

$$= \lim_{v \rightarrow v_0} \frac{(v - v_0) n(v)}{\bar{\theta}(v_0) + (v - v_0) \bar{\theta}'(v_0) + \frac{(v - v_0)^2}{2!} \bar{\theta}''(v_0) + \dots} \quad (104)$$

$$= \frac{n(v_0)}{\bar{\theta}'(v_0)}, \quad (105)$$

since $\bar{\theta}(v_0) = 0$ at the pole. Similarly,

$$C_M = \frac{n(v_M)}{\bar{\theta}'(v_M)}. \quad (106)$$

A 32-point Gauss quadrature evaluation of the nonsingular integral

$$\int_0^{2v_M} dv e^{-\gamma v} \left[f(v) - \frac{C_0}{v - v_0} - \frac{C_M}{v - v_M} \right] \quad (107)$$

compared well with 64-point Gauss quadrature evaluation in the sense that discrepancies between the two appeared at the 10th significant digit. It proved crucial to evaluate C_0 and C_M using analytical expressions for $\bar{\theta}'(v)$. Finite difference approximations gave poor results. The evaluation of the singular integrals must now be considered.

One can express the 1st of the singular integrals as follows:

$$\int_0^{2v_M} dv e^{-\gamma v} \frac{C_0}{v - v_0} = \int_0^{2v_0} dv e^{-\gamma v} \frac{C_0}{v - v_0} + \int_{2v_0}^{2v_M} dv e^{-\gamma v} \frac{C_0}{v - v_0}. \quad (108)$$

Taking into account that $|\gamma v_0| \ll 1$ for any conceivable transducer, and letting $W = \frac{v - v_0}{v_0}$, one is led to the excellent approximation that

$$\int_0^{2v_0} dv e^{-\gamma v} \frac{C_0}{v - v_0} \approx C_0 e^{-\gamma v_0} (-2\gamma v_0) + \dots \quad (109)$$

For the 2nd integral,

$$\int_{2U_0}^{2U_M} e^{-\gamma U} \frac{C_0}{U - U_0} = C_0 \int_1^{(2U_M - U_0)/U_0} \frac{e^{-\gamma U_0(1+w)}}{w} dw \quad (110)$$

$$= C_0 e^{-\gamma U_0} \{E_1[\gamma U_0] - E_1[\gamma(2U_M - U_0)]\}. \quad (111)$$

Collecting terms one finally arrives at

$$\int_0^{2U_M} e^{-\gamma U} \frac{C_0}{U - U_0} = C_0 \{-2\gamma U_0 + E_1[\gamma U_0] - E_1[\gamma(2U_M - U_0)]\} e^{-\gamma U_0} \quad (112)$$

The other singular integral was cast into the form

$$\int_0^{2U_M} e^{-\gamma U} \frac{C_M}{U - U_M} = C_M e^{-\gamma U_M} \int_{-1}^1 \frac{e^{-\gamma U_M w}}{w} dw, \quad (113)$$

which was easily and accurately evaluated using an even-point Gauss quadrature.

This completes the evaluation of the integral

$$\int_0^{2U_M} e^{-\gamma U} f(U). \quad (114)$$

2.7 Integration Over the Semi-infinite Interval $(2U_M, \infty)$

For a line current residing on the YIG film, the integrand can fall off as slowly as $1/U$ for large U . We therefore "subtracted off" the asymptotic behavior of the integrand and then "added" its effect back into the final

answer as shown:

$$\int_{2U_M}^{\infty} du e^{-\gamma u} f(u) = \int_{2U_M}^{\infty} du e^{-\gamma u} \underbrace{\left[f(u) + \frac{1}{u} \right]}_{g(u)} - \int_{2U_M}^{\infty} du \frac{e^{-\gamma u}}{u} \quad (115)$$

$$= \int_{2U_M}^{\infty} du e^{-\gamma u} g(u) - E_1[2U_M \gamma] \quad (116)$$

$$= \int_{2U_M}^{\infty} du e^{-\gamma u} [g(u) - g_{\infty}(u)] + \int_{2U_M}^{\infty} du e^{-\gamma u} g_{\infty}(u) \quad (117)$$

$$- E_1[2U_M \gamma].$$

$g_{\infty}(u)$ is an asymptotic form of $g(u)$ and its use as indicated above speeds the convergence of the integral. Since

$$g(u) \equiv f(u) + \frac{1}{u} \quad (118)$$

$$= \frac{U g_{\pm}}{\bar{B}(u)} + \frac{\bar{B}(\infty)}{u \bar{B}(u)} \quad (119)$$

it follows, after some algebra, that

$$g_{\infty}(u) = \frac{[U g_{\pm} + \bar{B}(\infty) u^{-1}] \bar{B}_{\infty}^{-1}}{u^2 - E_{\infty} \bar{B}_{\infty}^{-1}} \quad (120)$$

where

$$E_{\infty} = (1 - |\bar{b}|) |\bar{b}| U_s^2 \quad (121)$$

and

$$\bar{\Theta}_{\infty} = (1 + \bar{e}^2 + \bar{b}^2 + 2\bar{b}). \quad (122)$$

It can be seen that $g_{\infty}(U)$ is expandable in partial fractions and that one is led to

$$\int_{2U_M}^{\infty} dU e^{-\gamma U} g_{\infty}(U) = F_1 E_1[2\gamma U_M] + F_2 \left\{ e^{-\gamma F_3} E_1[\gamma(2U_M - F_3)] + e^{\gamma F_3} E_1[\gamma(2U_M + F_3)] \right\} \quad (123)$$

where

$$F_1 = -\bar{\Theta}_{(0)} / E_{\infty} \quad (124)$$

$$F_2 = \frac{1}{2} [g_{\pm} \bar{\Theta}_{\infty}^{-1} + \bar{\Theta}_{(0)} E_{\infty}^{-1}] \quad (125)$$

and

$$F_3 = \sqrt{E_{\infty} \bar{\Theta}_{\infty}^{-1}}. \quad (126)$$

2.8 Half-Period Integration

The only integral remaining to be evaluated is

$$I = \int_{2U_M}^{\infty} dU e^{-\gamma U} [g(U) - g_{\infty}(U)]. \quad (127)$$

Let

$$Q(U) = g(U) - g_{\infty}(U) \quad (128)$$

$$U = \varphi / |\bar{x} / U_M| + 2U_M, \quad (129)$$

and replace γ with $(\bar{\beta} - i|\bar{x}|)/U_M$ in the integral.

This leads to

$$I = \frac{U_M}{|\bar{x}|} e^{-2(\bar{\beta} - i|\bar{x}|)} \int_0^{\infty} d\varphi e^{-\frac{\bar{\beta}}{|\bar{x}|}\varphi} e^{i\varphi} Q[U(\varphi)]. \quad (130)$$

The procedure adopted for its evaluation was to integrate over N half-periods of the sine and cosine functions integrals separately. 4 sets of partial sums were thus obtained:

$$1.) \int_0^{\infty} d\varphi (\sin \varphi) Q \dots = \begin{cases} \text{left half-period integrations} \\ \text{right half-period integrations} \end{cases} \quad (131)$$

and

$$2.) \int_0^{\infty} d\varphi (\cos \varphi) Q \dots = \begin{cases} \text{left half-period integrations} \\ \text{right half-period integrations} \end{cases} \quad (132)$$

Each sequence of partial sums was then extrapolated to $N \rightarrow \infty$ using a Shank's transformation [Ref. 9]. A modified Shank's transformation, was actually implemented [Ref. 10] but it did not do better than the simpler version.

With

$$\varphi = \theta + (n-1)\pi \quad (133)$$

$$0 \leq \theta < \pi \quad \text{and} \quad n = 1, 2, \dots, N$$

it follows that

$$I = \frac{U_M}{|\bar{x}|} e^{-2(\bar{\beta} - i|\bar{x}|)} \sum_{n=1}^{N \rightarrow \infty} \int_0^{\pi} d\theta e^{-\frac{\bar{\beta}}{|\bar{x}|}[\theta + (n-1)\pi]} \cdot e^{i[\theta + (n-1)\pi]} Q[U(\varphi(\theta))], \quad (134)$$

showing that each term in the partial sum involves a half-period. For the actual computations over each half cycle, it was useful to let $\theta \equiv \frac{\pi}{2} (t + 1)$

so that

$$I = i \frac{\pi}{2} \frac{U_n}{|\bar{x}|} e^{-2\gamma U_n} \sum_{n=1}^{N \rightarrow \infty} (-1)^{n-1} e^{-\frac{\bar{\beta}}{|\bar{x}|} (2n-1)} \int_{-1}^1 dt e^{i \frac{\pi}{2} t} e^{-\frac{\pi}{2} \frac{\bar{\beta}}{|\bar{x}|} t} \cdot Q[U(n, t)], \quad (135)$$

where

$$U = \frac{\pi}{|\bar{x}/U_n|} \left[n + \frac{1}{2}(t-1) \right] + 2U_n. \quad (136)$$

Each integral was calculated using 32-point Gauss quadrature. The total expression for $Q^{(1)}$ is thus given by

$$\begin{aligned} Q^{(1)} = & \ln[x^2 + (y-d)^2] - \frac{1}{2} \ln[x^2 + (y+d)^2] + i t_n^{-1} \left(\frac{|\bar{x}|}{y+d} \right) \\ & + C_0 e^{-\gamma U_0} \left\{ -2\gamma U_0 + E_1[\gamma U_0] - E_1[\gamma(2U_n - U_0)] \right\} \\ & + C_n e^{-\gamma U_n} \int_{-1}^1 dw \frac{e^{-\gamma U_n w}}{w} + \int_0^{2U_n} dv e^{-\gamma v} \left[f(v) - \frac{C_0}{v-U_0} - \frac{C_n}{v-U_n} \right] \\ & + (F_1 - 1) E_1[2\gamma U_n] + F_2 \left\{ e^{-\gamma F_2} E_1[\gamma(2U_n - F_2)] + e^{\gamma F_2} E_1[\gamma(2U_n + F_2)] \right\} \\ & + i \frac{\pi}{2} \frac{U_n}{|\bar{x}|} e^{-2\gamma U_n} \sum_{n=1}^{N \rightarrow \infty} (-1)^{n-1} e^{-\frac{\bar{\beta}}{|\bar{x}|} (2n-1)} \int_{-1}^1 dt e^{i \frac{\pi}{2} t} e^{-\frac{\pi}{2} \frac{\bar{\beta}}{|\bar{x}|} t} Q[U(t, n)]. \end{aligned} \quad (137)$$

2.9 Results and Discussion

The quantity \mathcal{A}^{\odot} , the normalized Green's function, was programmed and put through a series of tests. As Fig. 2.3-2.21 shows, the Green's function has real and imaginary parts as depicted by solid and dashed lines respectively. The real and imaginary components are off by a physically irrelevant complex constant in the figure. The amplitude in the $-x$ direction is larger than in the $+x$ direction, as would be expected based on the direction of $\underline{H}_0 \times \hat{n}$. See Fig. 2-1 and [Ref. 8]. Furthermore, the $\pm x$ amplitudes are not uniform. From the tests we were able to perform, this does not appear to be numerical error: there seems to be a small, spatially dependent transient near the line source at the origin. At large distances from the source, harmonic surface waves dominate; very near the source, as seen in Fig. 2.2, there is a logarithmic variation in the field, as well as discontinuity at the source; and between the two extremes a region of transition.

For distances of 150 microns or less from the source, and using the same parameters noted earlier, the integral I in (127) was found to be negligible. At considerably larger distances the half-period integrations and extrapolations become important: the algorithm showed convergence to 9 or 10 significant digits at distances of about λ_M or less; whereas, at $3 \lambda_M$ 6-8 significant digits were obtained for I at several frequencies. For large distances, pure harmonic surface waves of the form

$$S_z e^{i[k_M |x| - \omega t - \pi/4]} \quad (138)$$

strongly dominate the Green's function.

The usefulness of the Green's function for calculating the surface current distributions on one or more strips depends to a large measure on the

time, i.e., expense, of its computation. For a given frequency and a given distance (positive or negative) of the field point from the line source, it took less than 0.15 seconds to evaluate the Green's function. Additional programming refinements and/or a loosening of some of the accuracy tolerances would reduce the computation time even further; however, the program appears to be a useful tool in its present form especially when used in conjunction with a cubic spline interpolation code. The next stage of work is to implement the Green's function for obtaining the current density on a strip residing on the YIG. This involves inverting an integral equation, and is in progress.

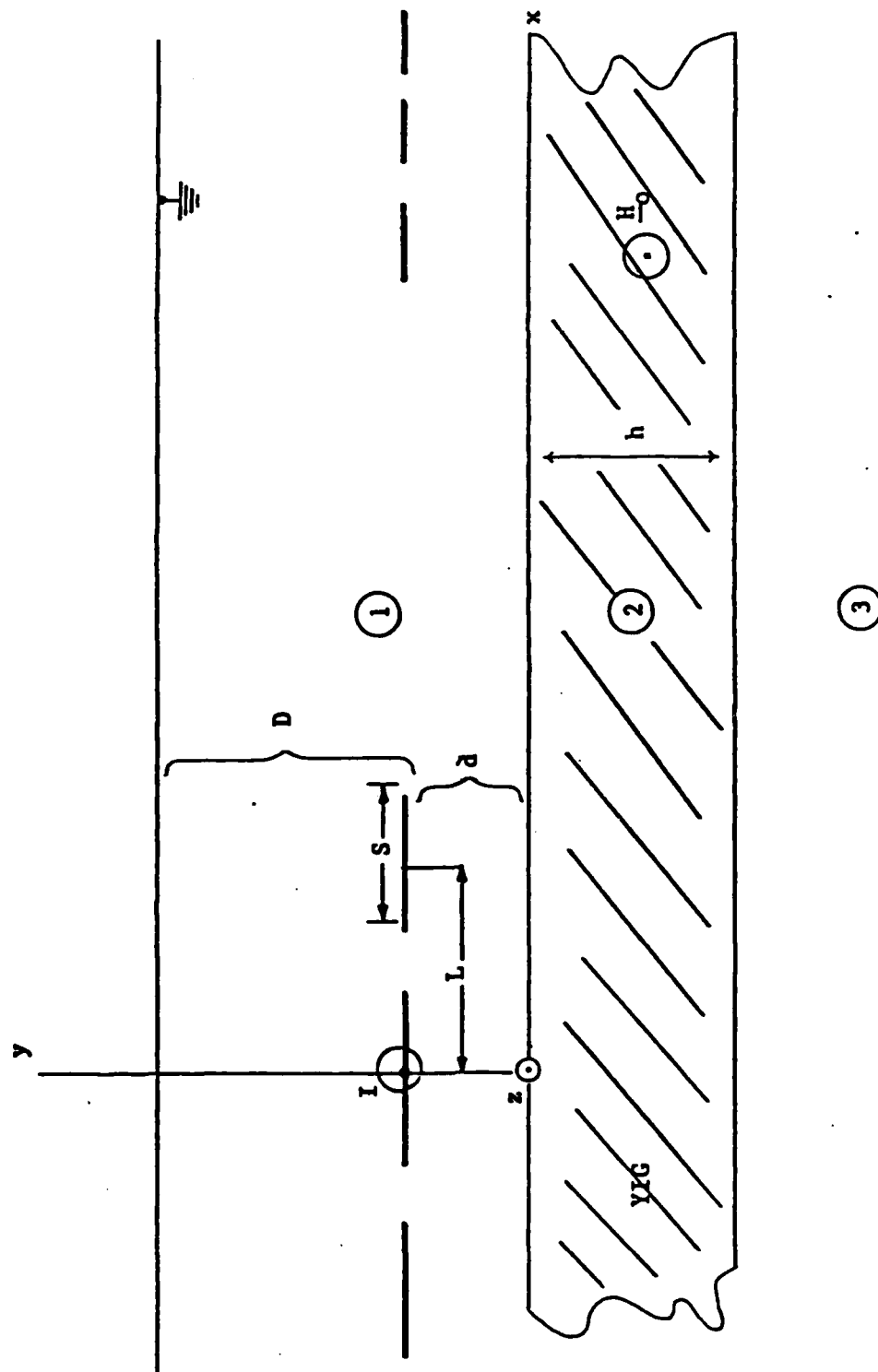


Fig. 2.1 Transducer Geometry

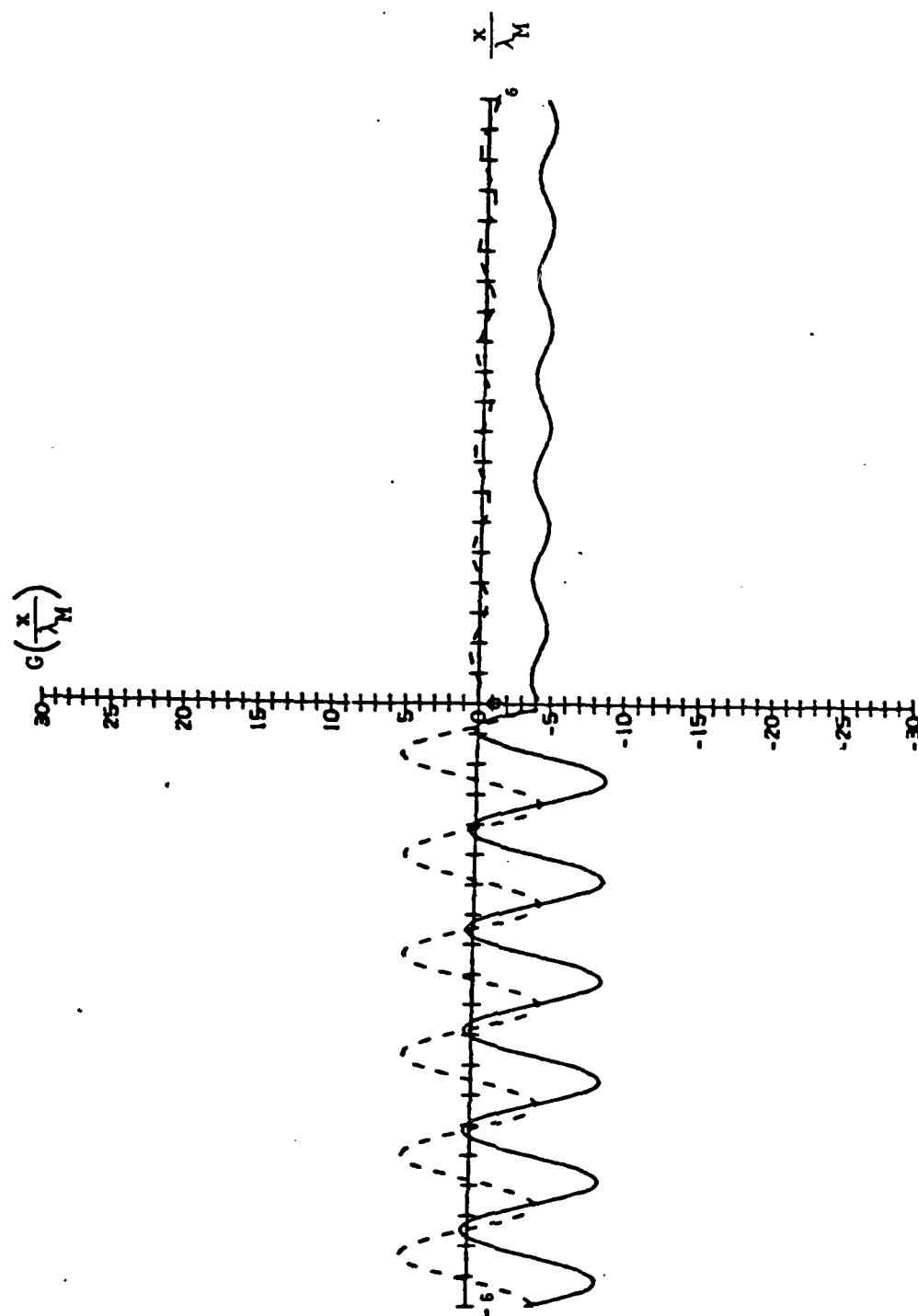


Fig. 2.2 Green's Function at $f = 2.8$ Ghz
for x/λ_M large.

Green's Function

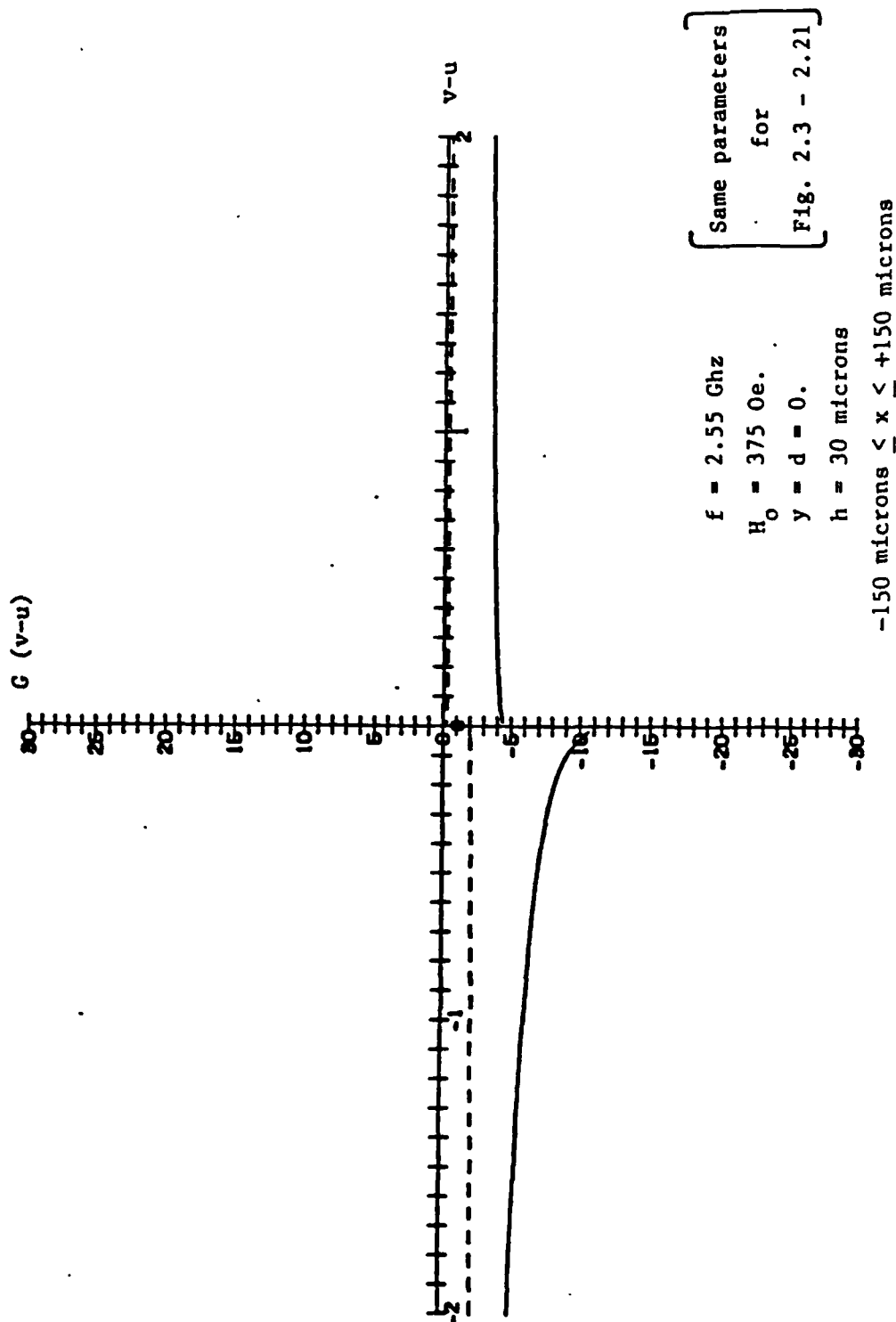


Fig. 2.3

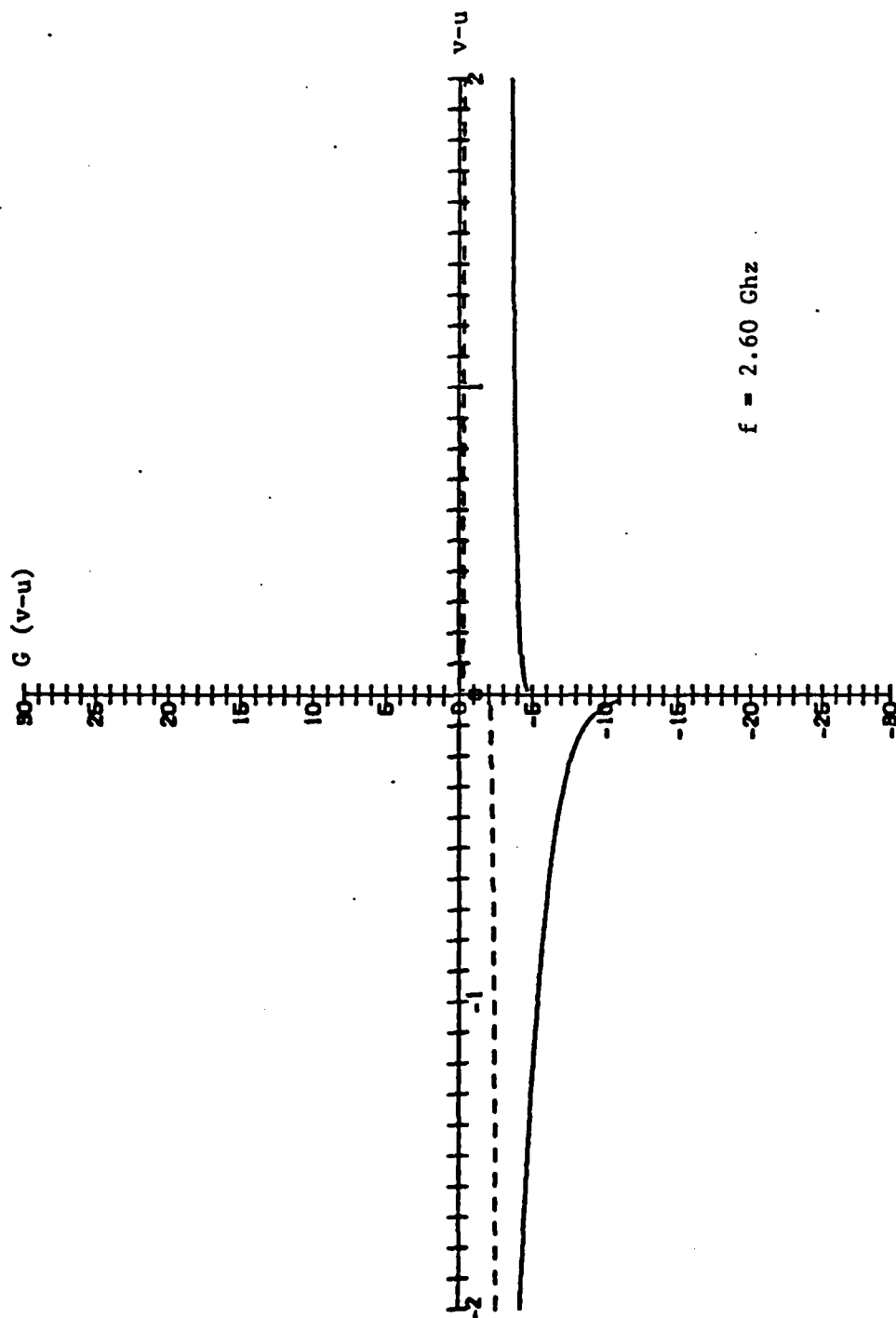


Fig. 2.4

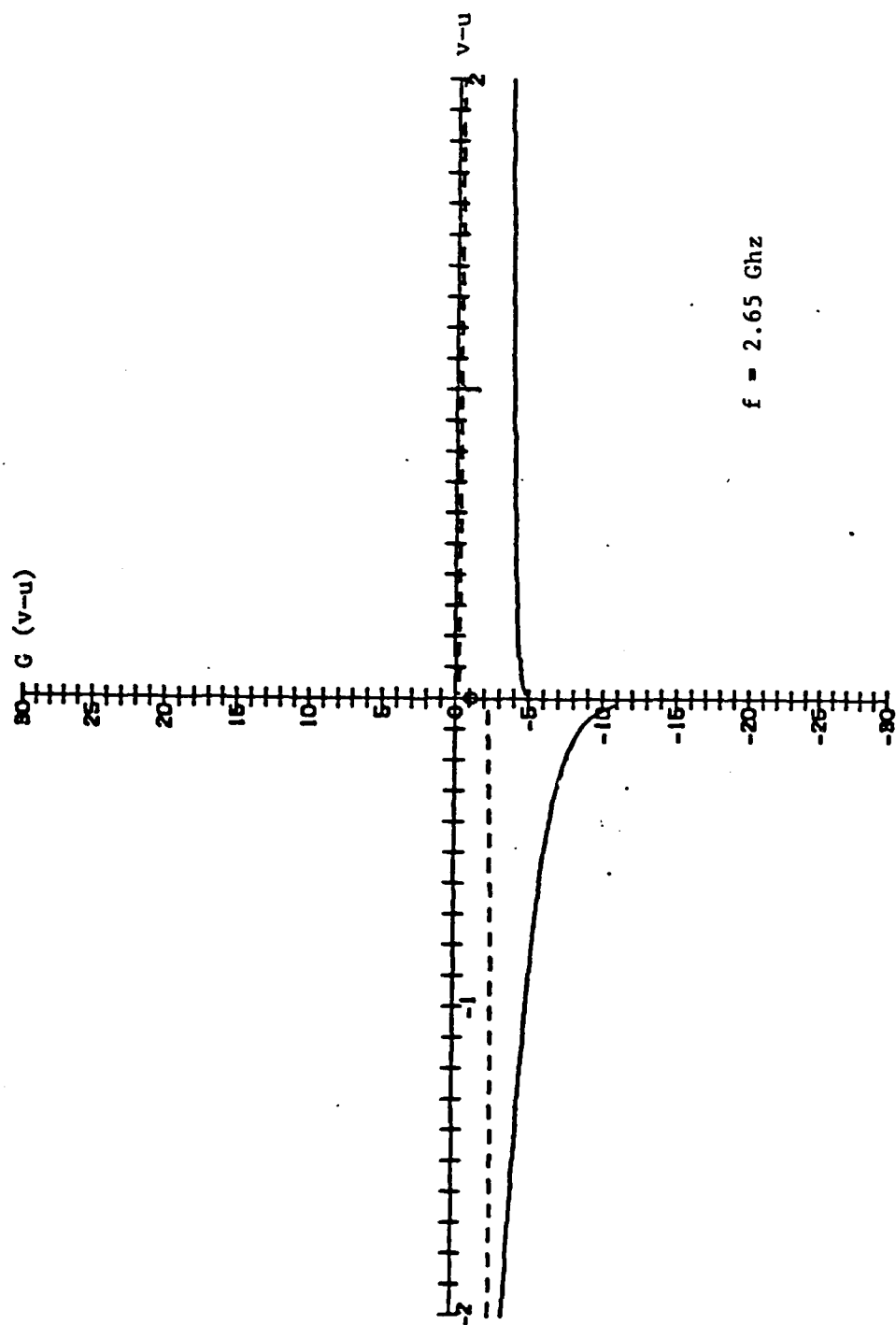


Fig. 2.5

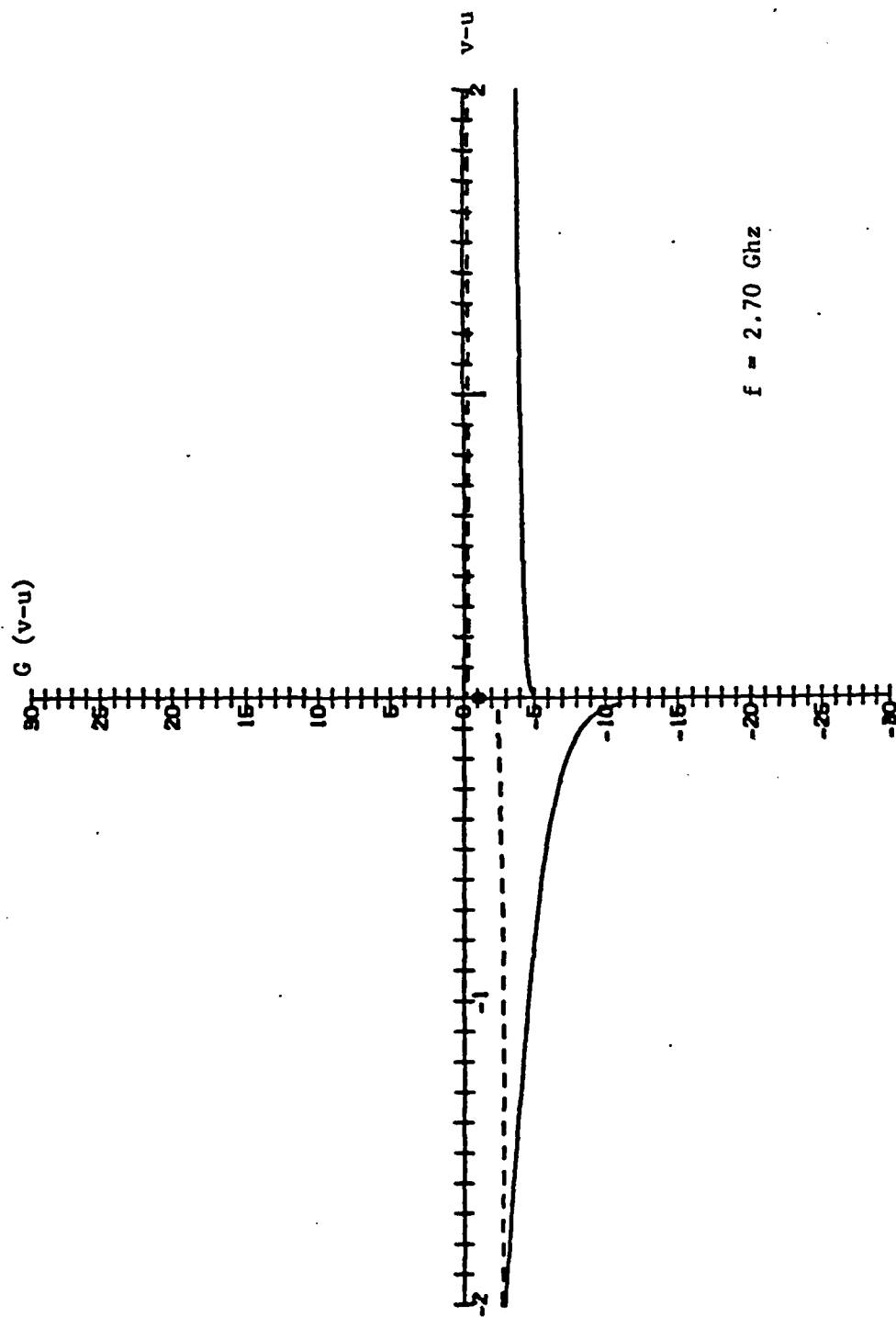
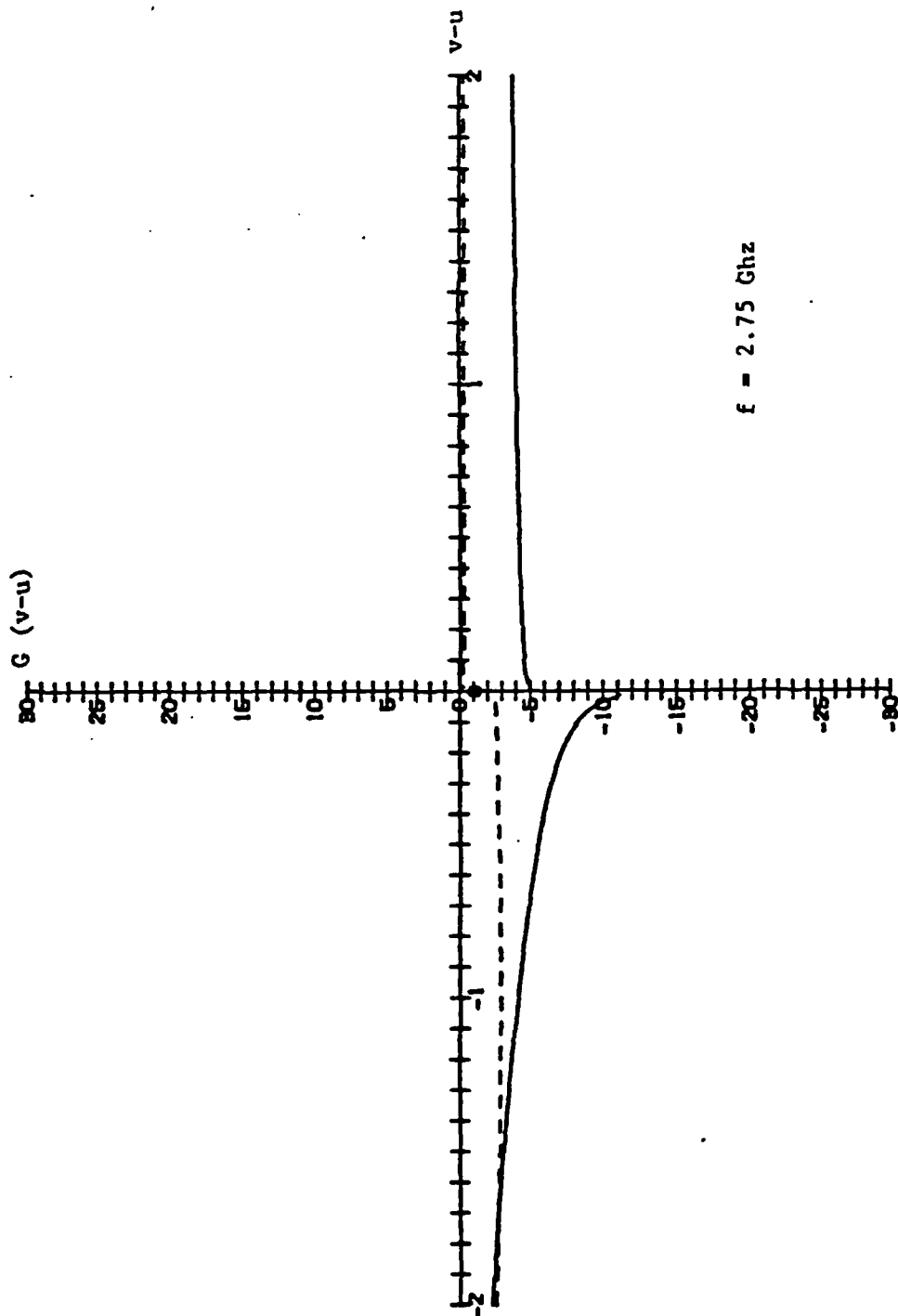


Fig. 2.6



$f = 2.75 \text{ GHz}$

Fig. 2.7

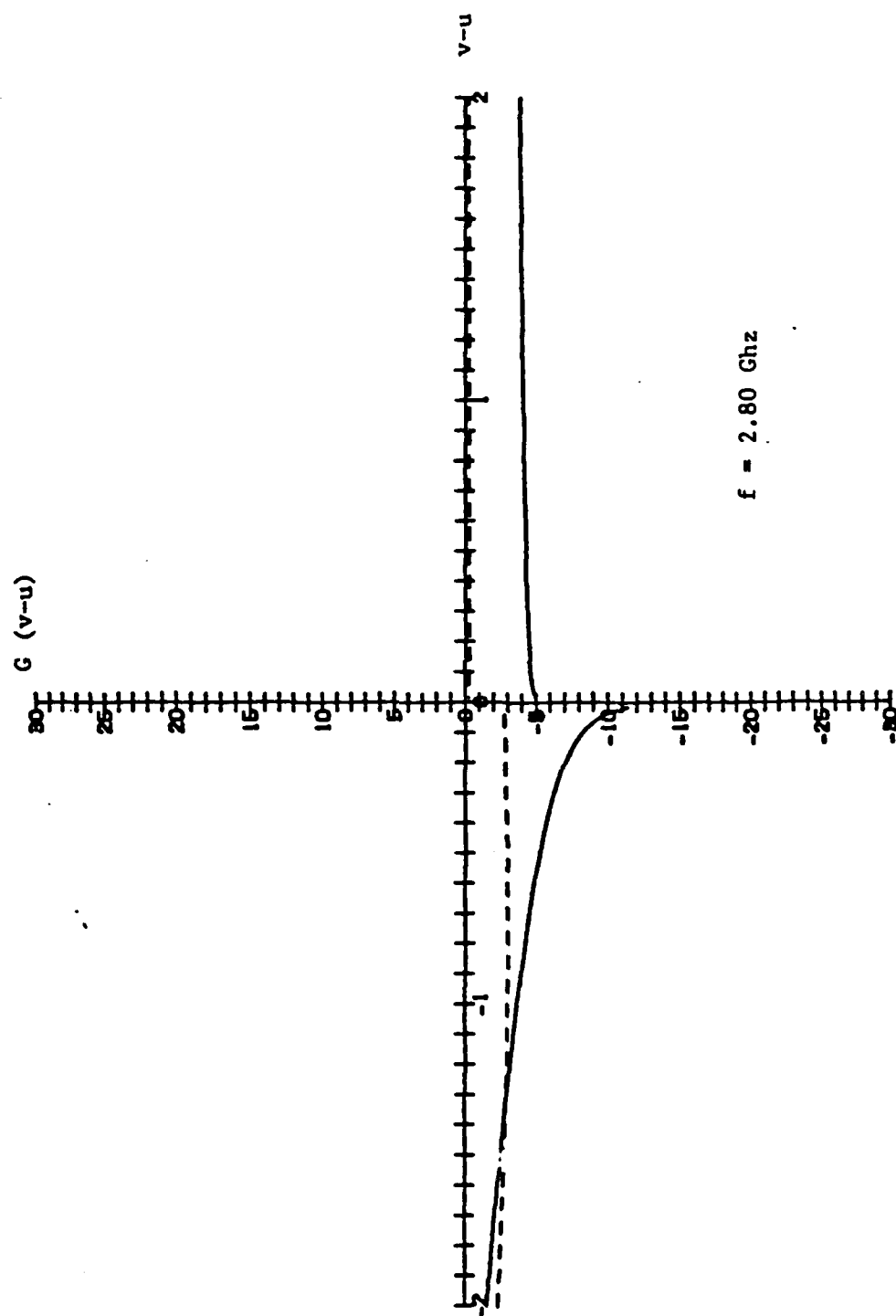


Fig. 2.8

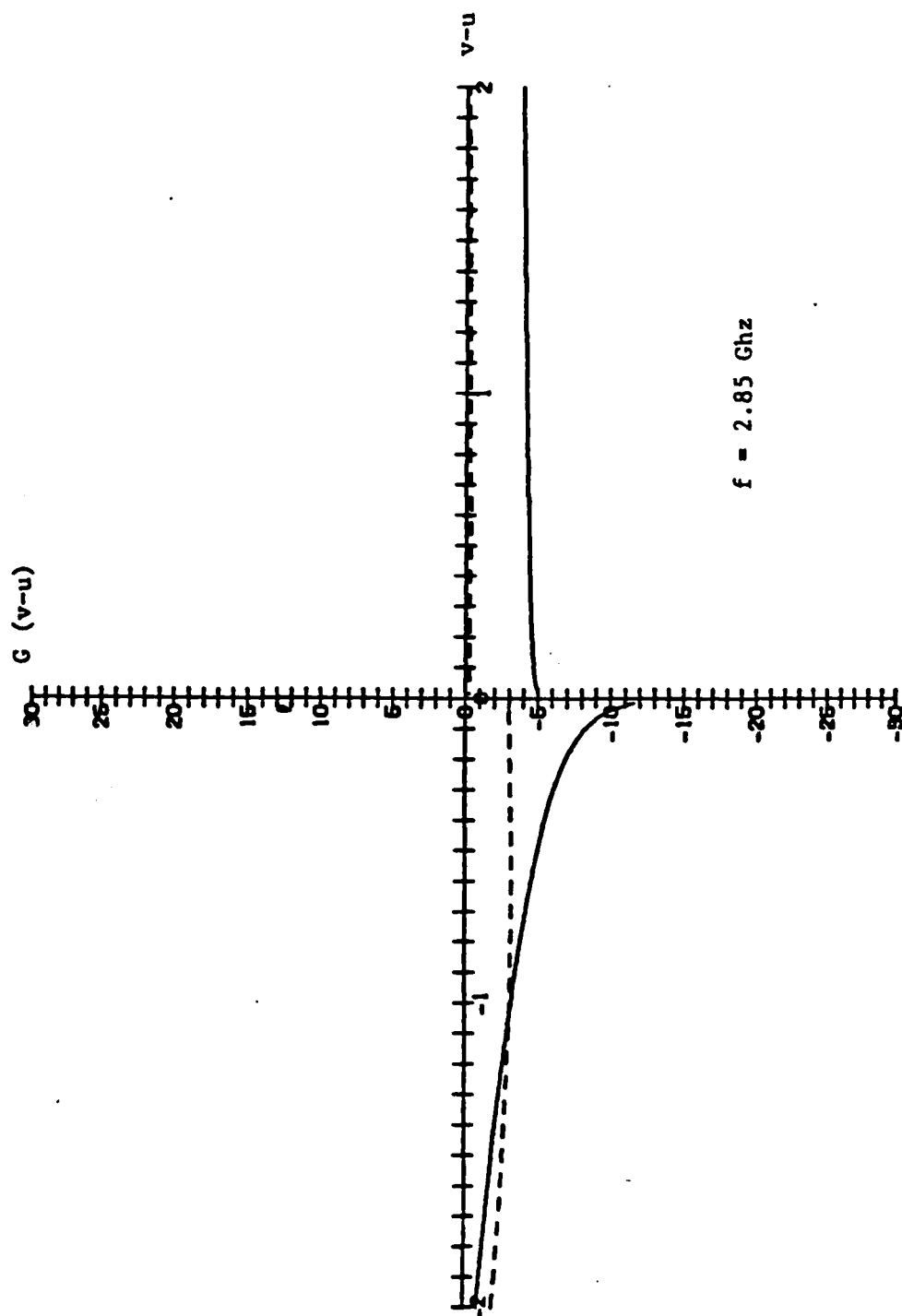


Fig. 2.9

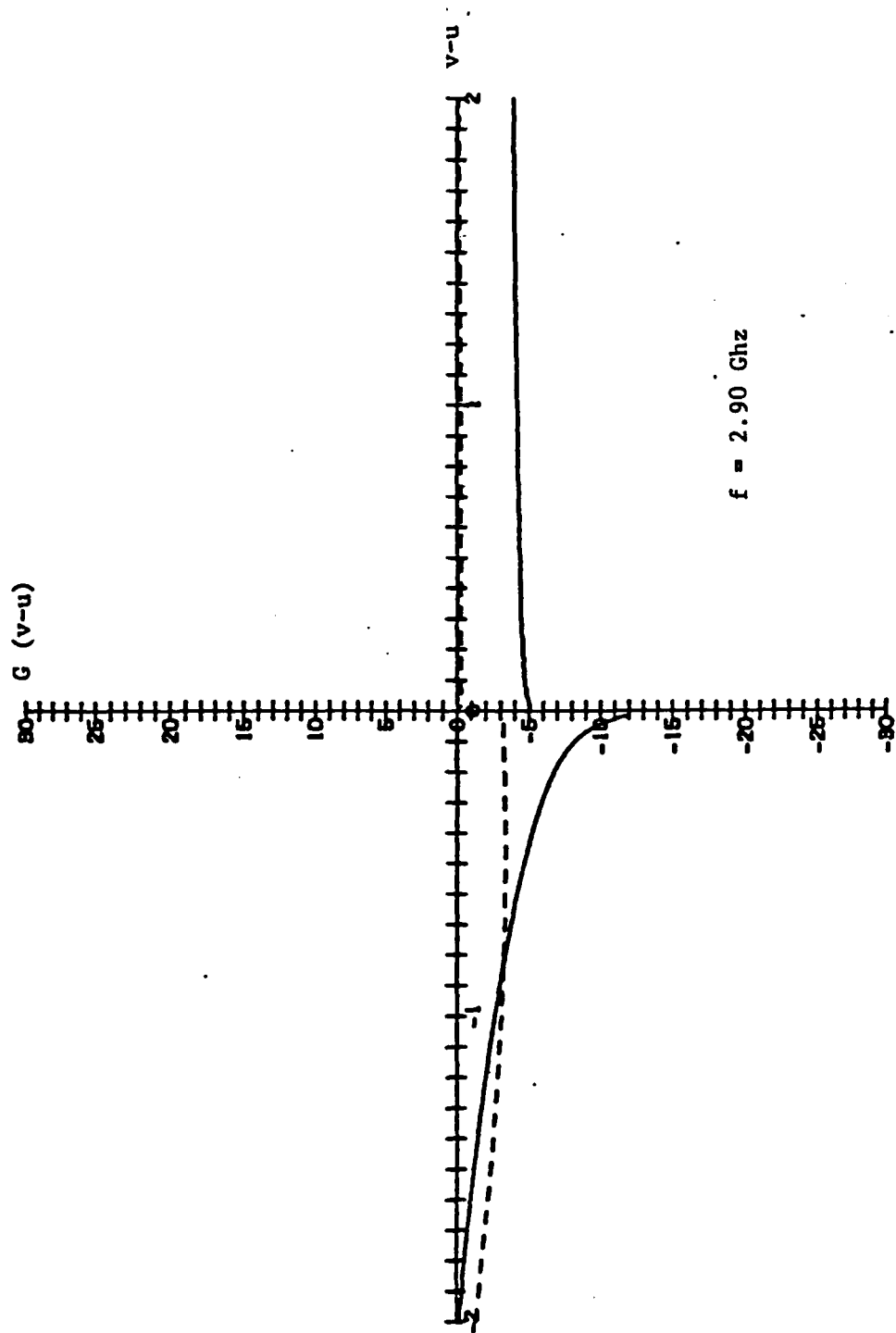


Fig. 2.10

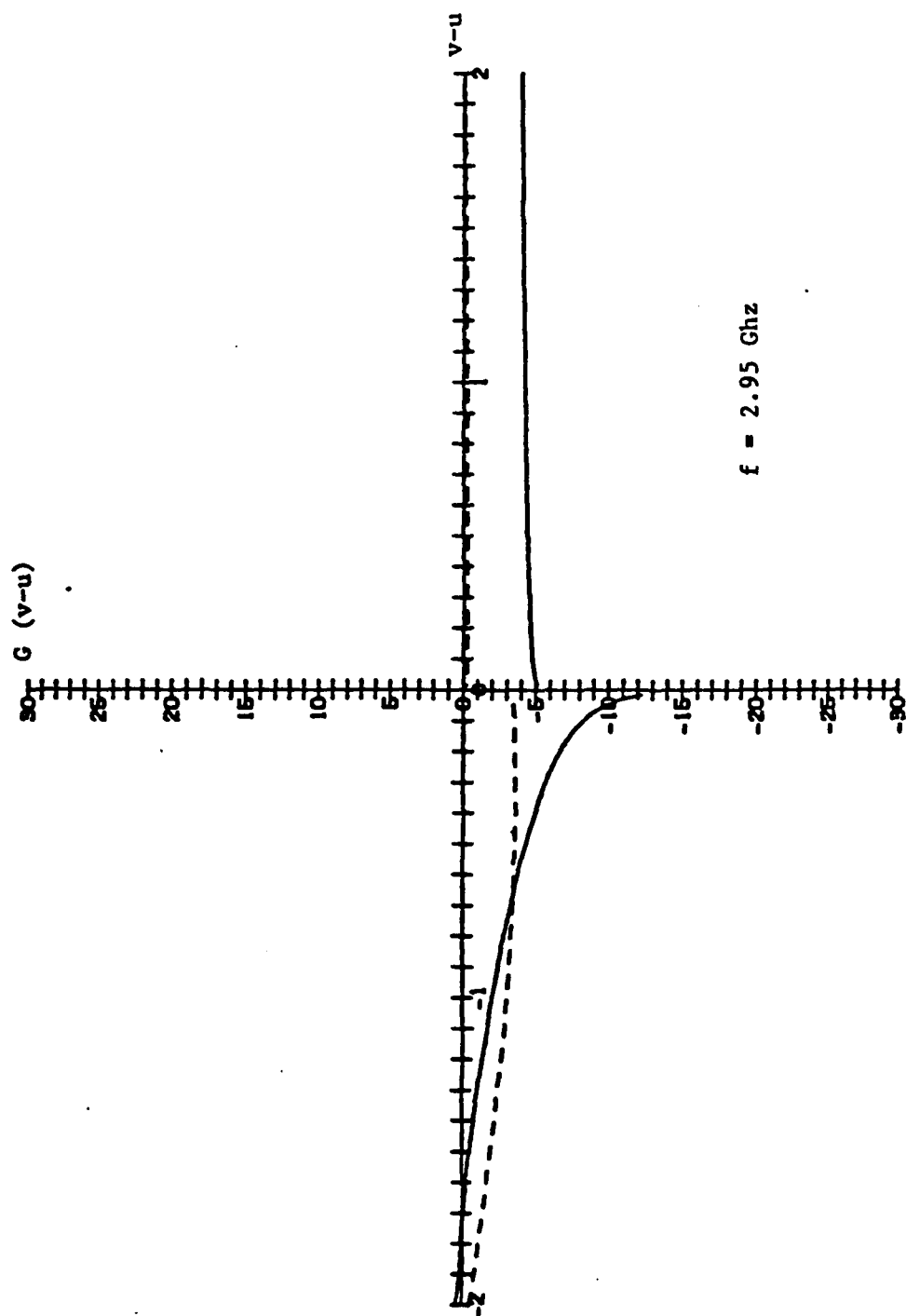
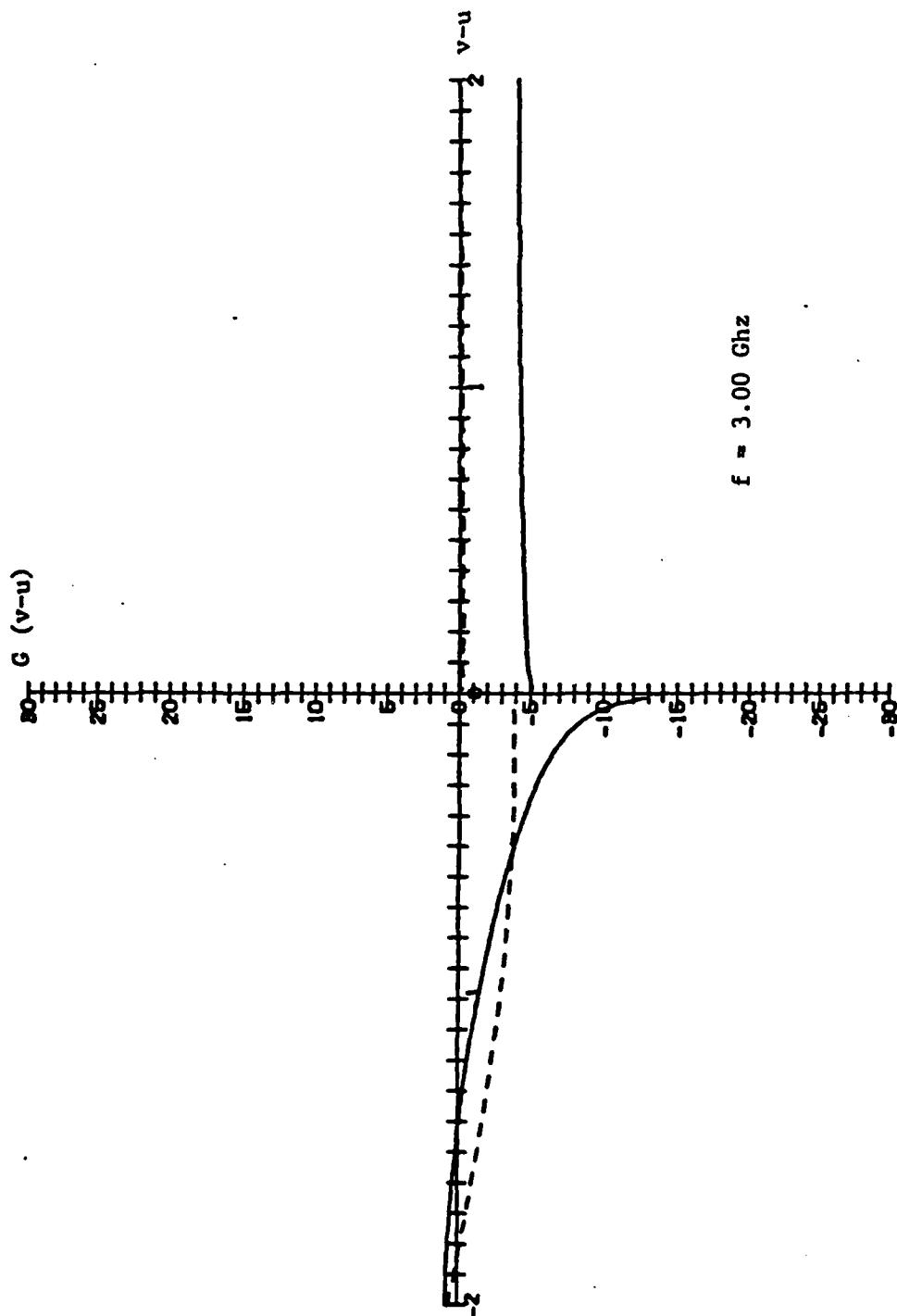


Fig. 2.11



$f = 3.00 \text{ GHz}$

Fig. 2.12

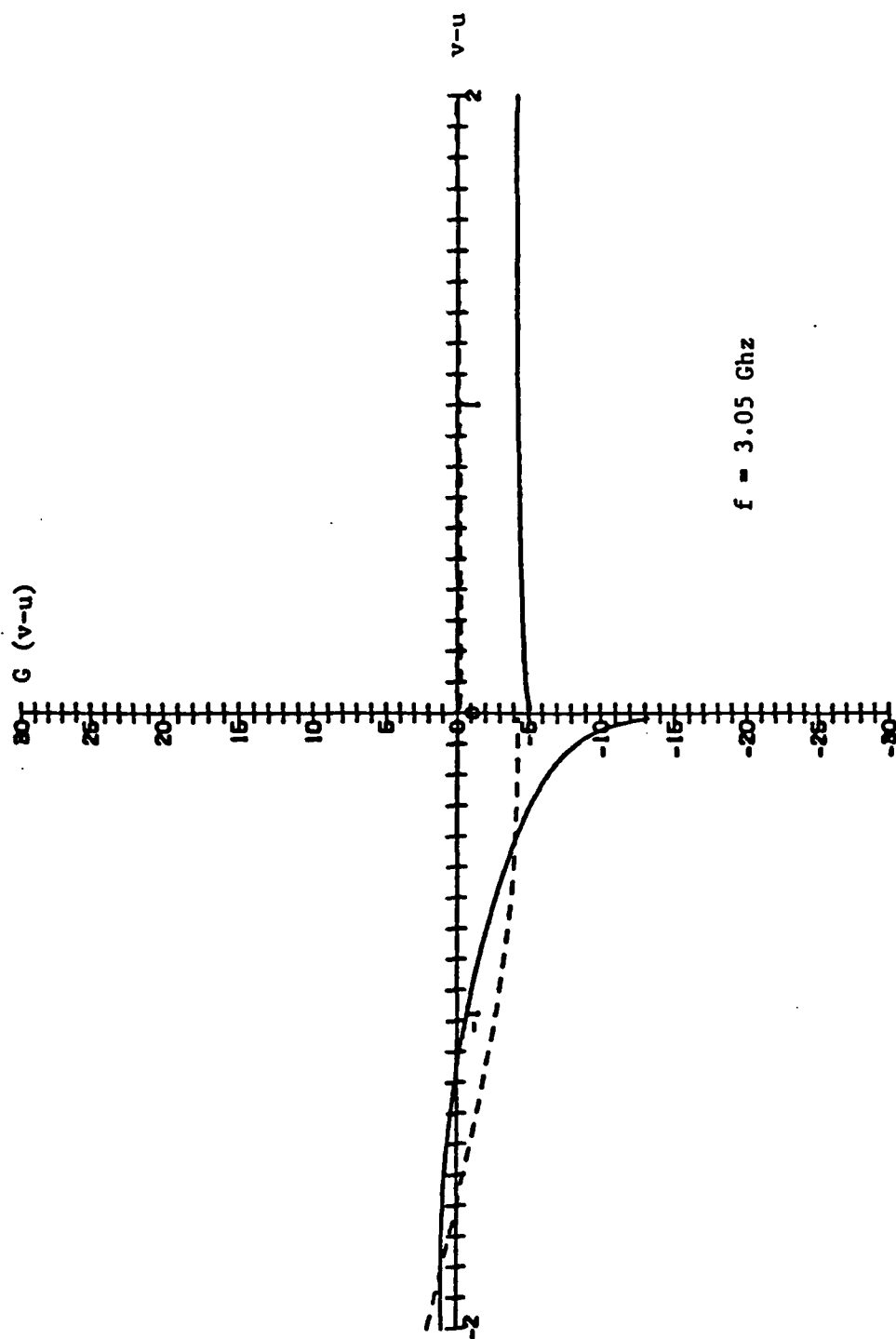


Fig. 2.13

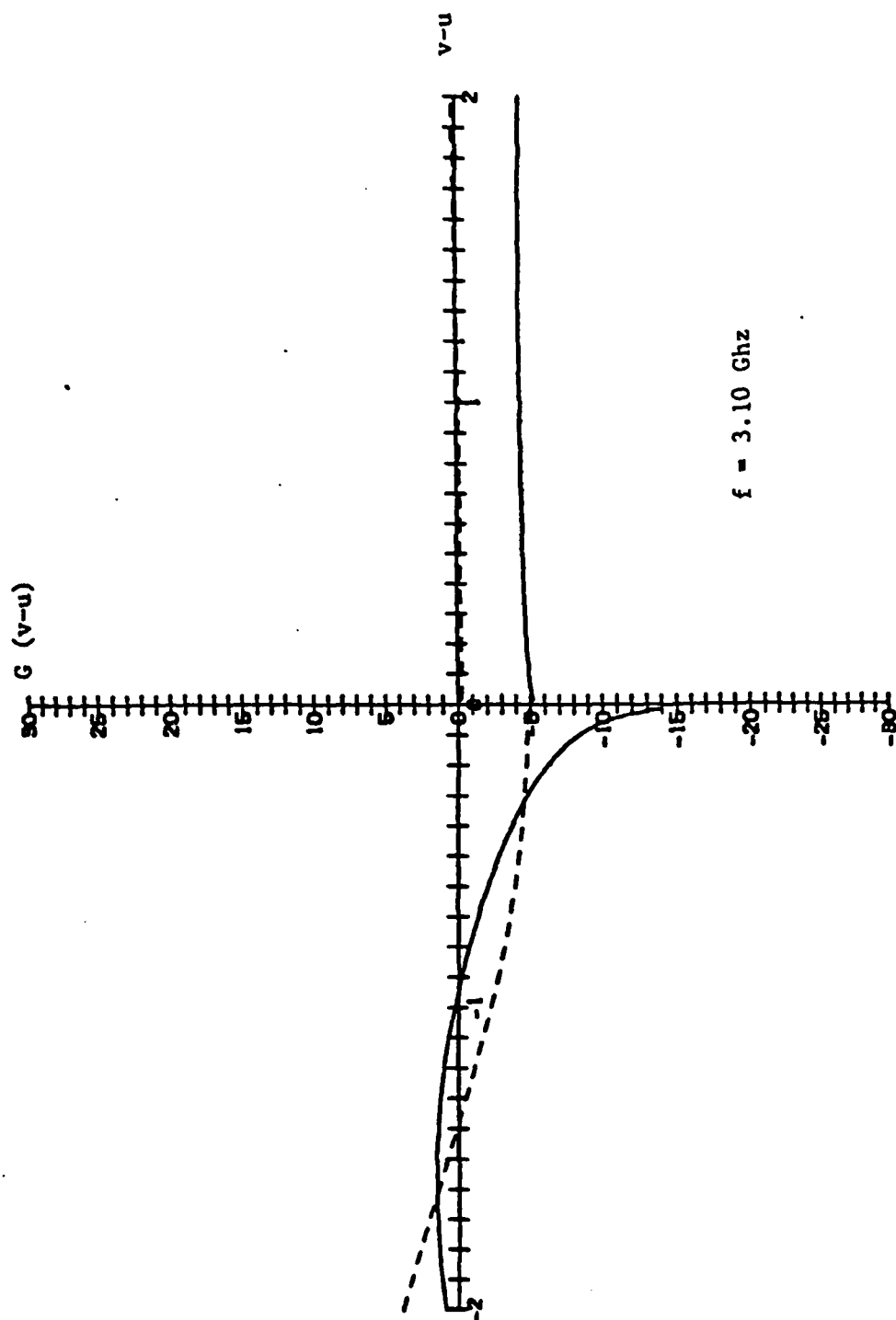


Fig. 2.14

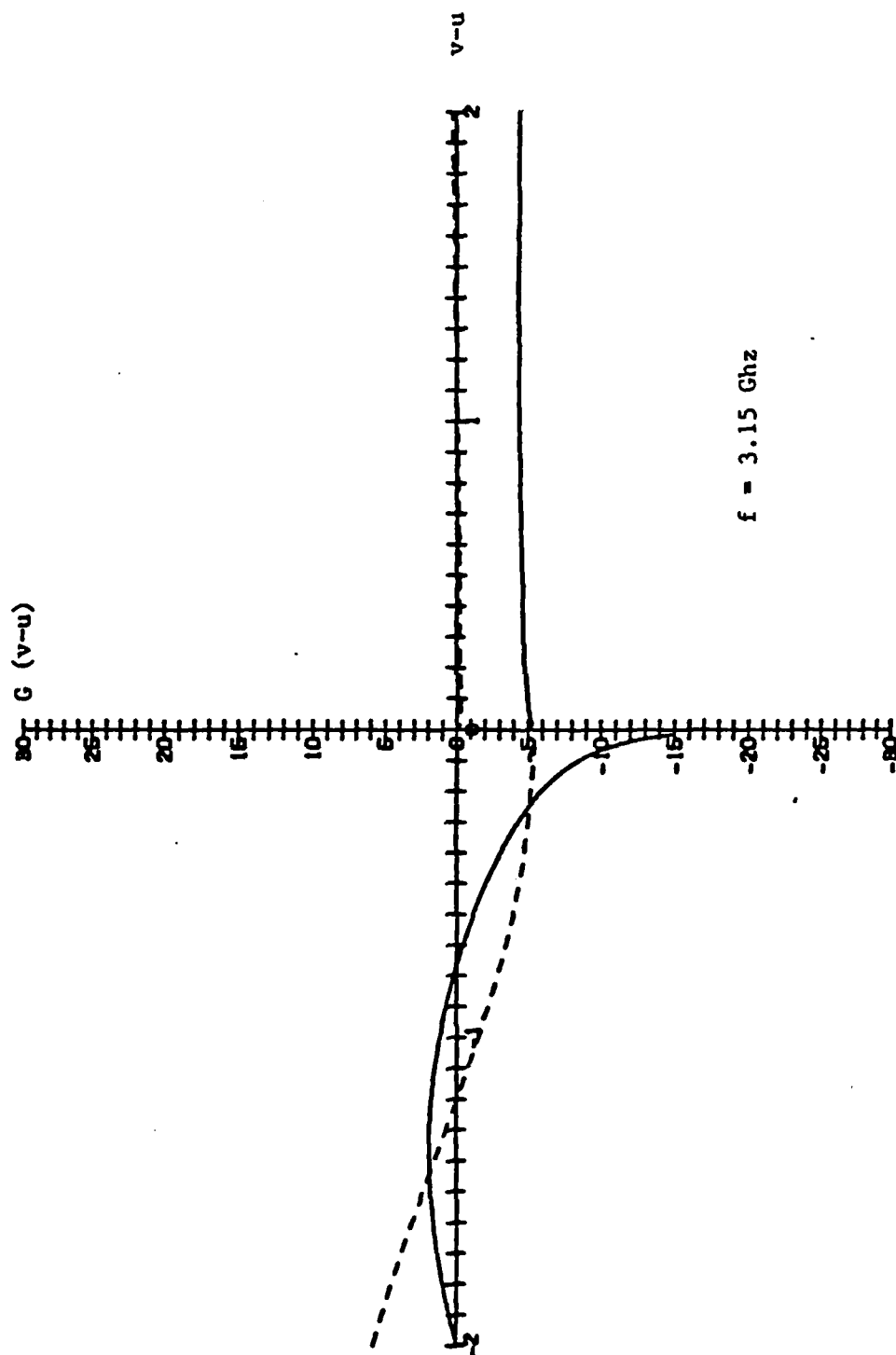


Fig. 2.15

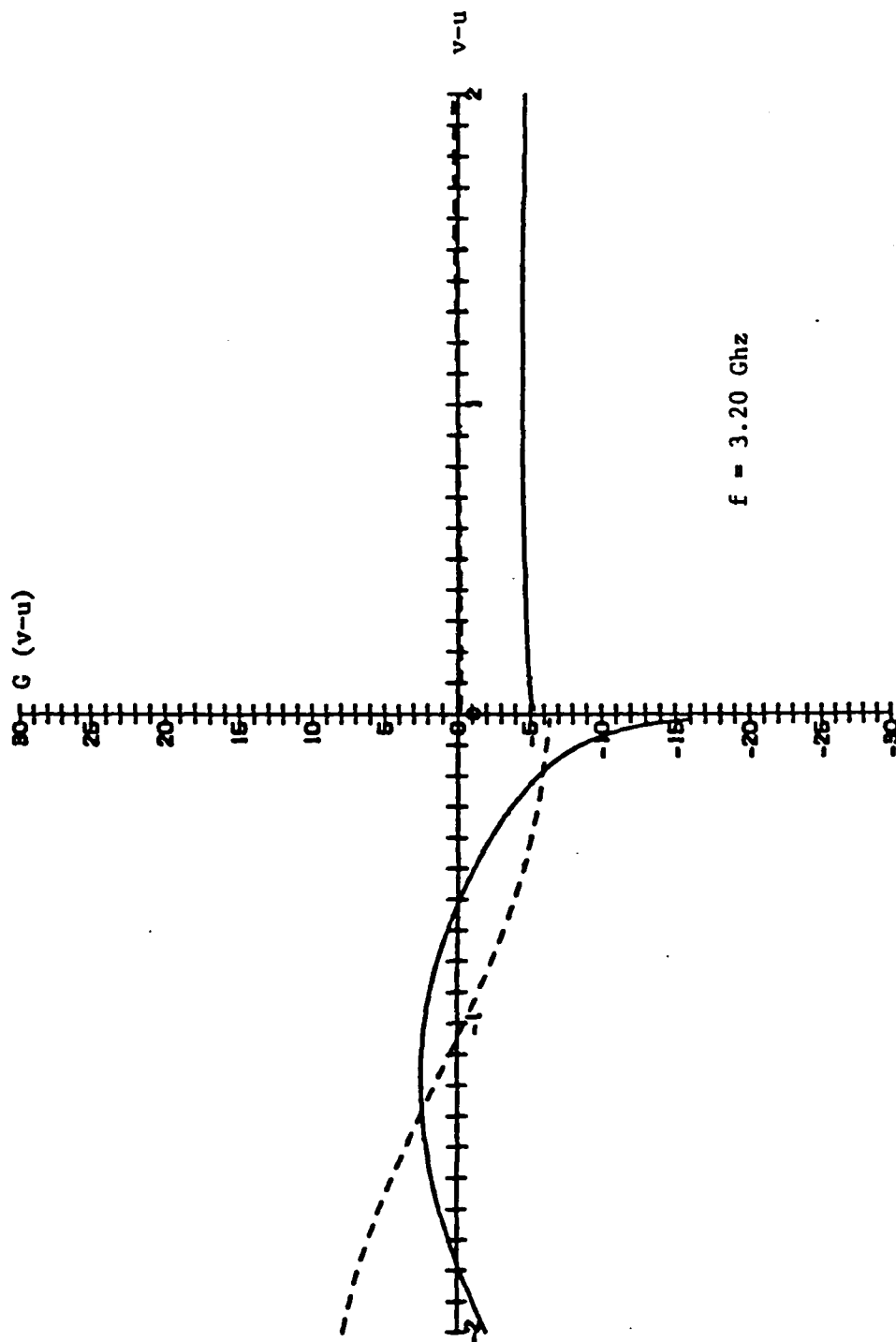


Fig. 2.16

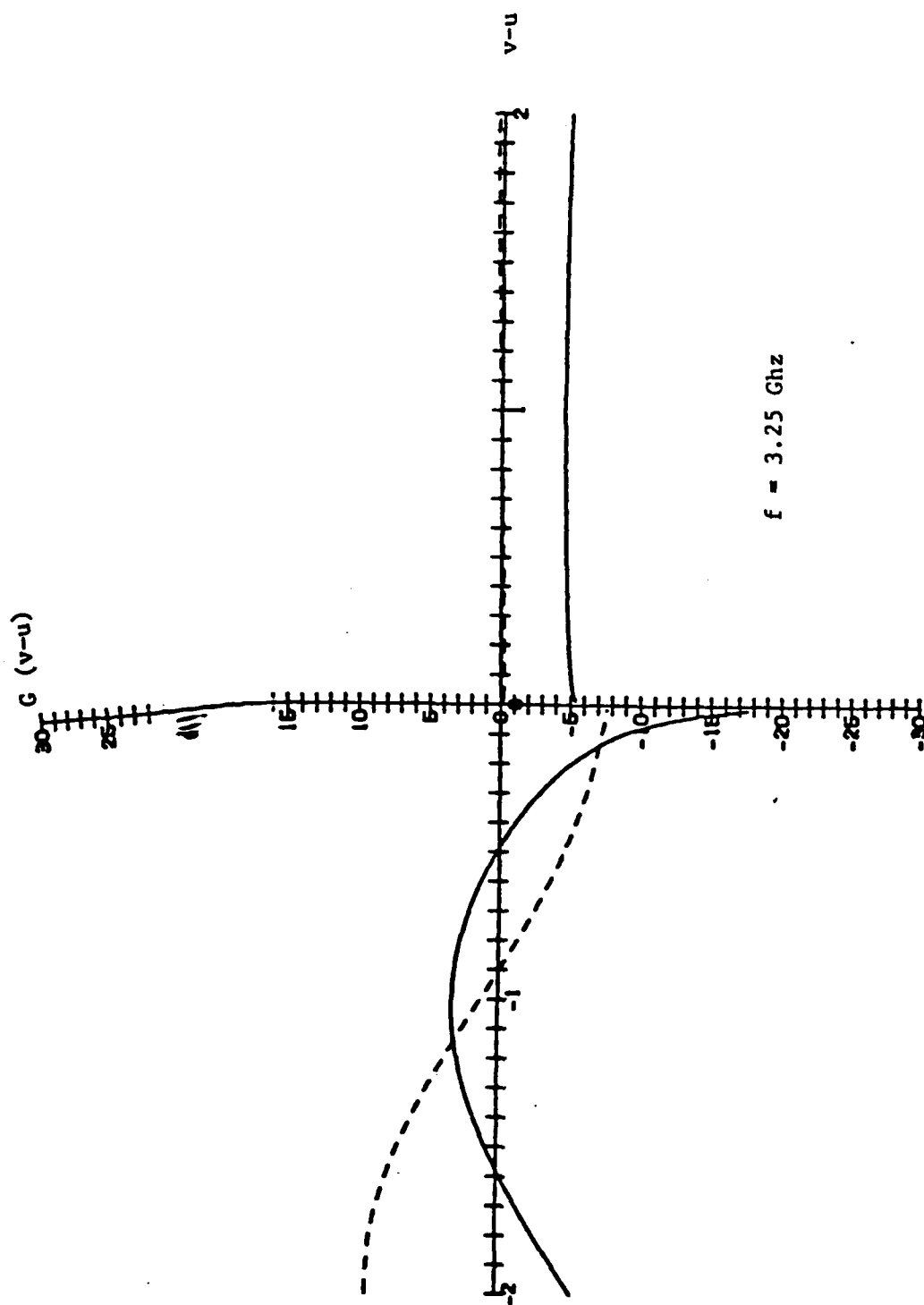


Fig. 2.17

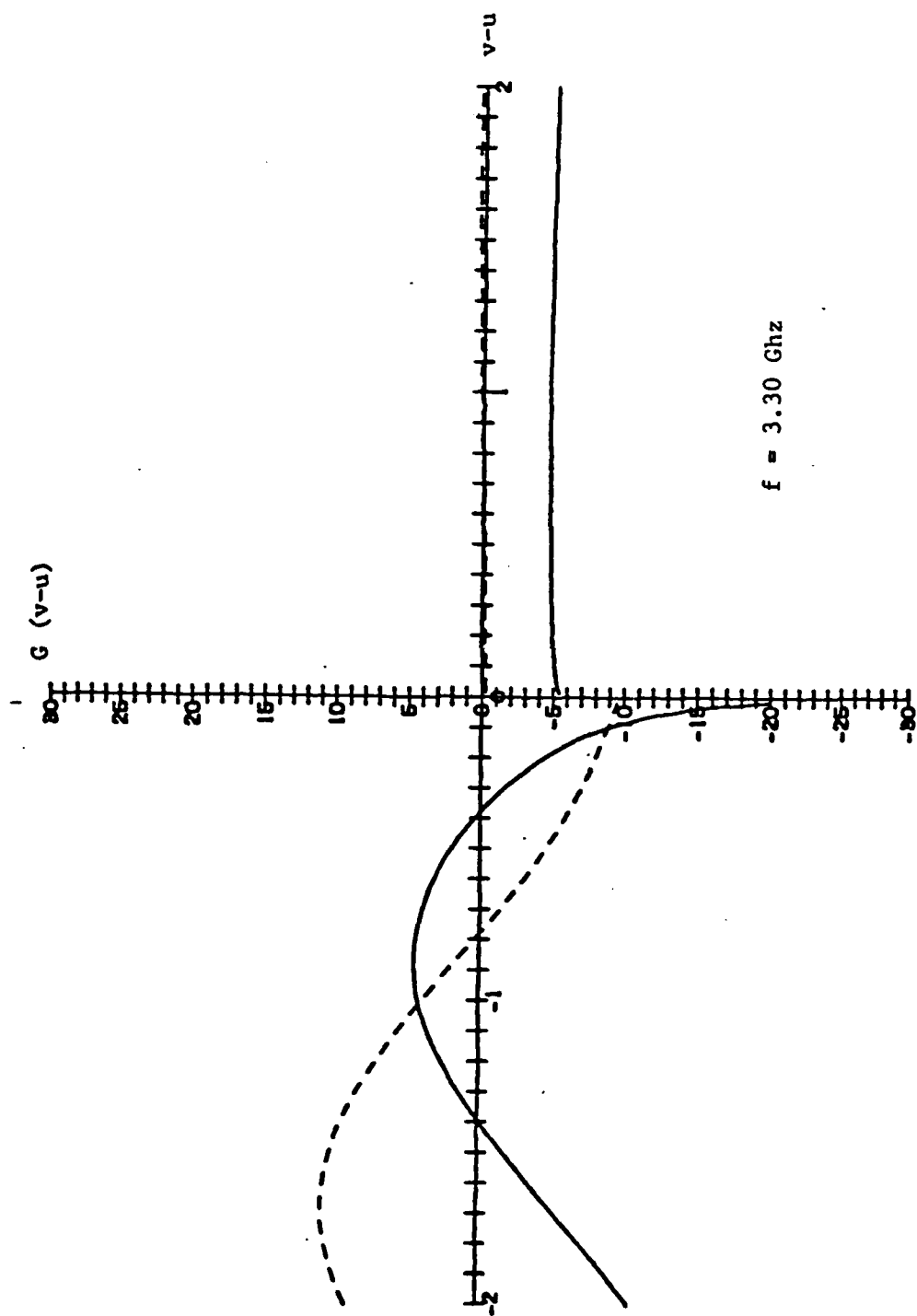


Fig. 2.18

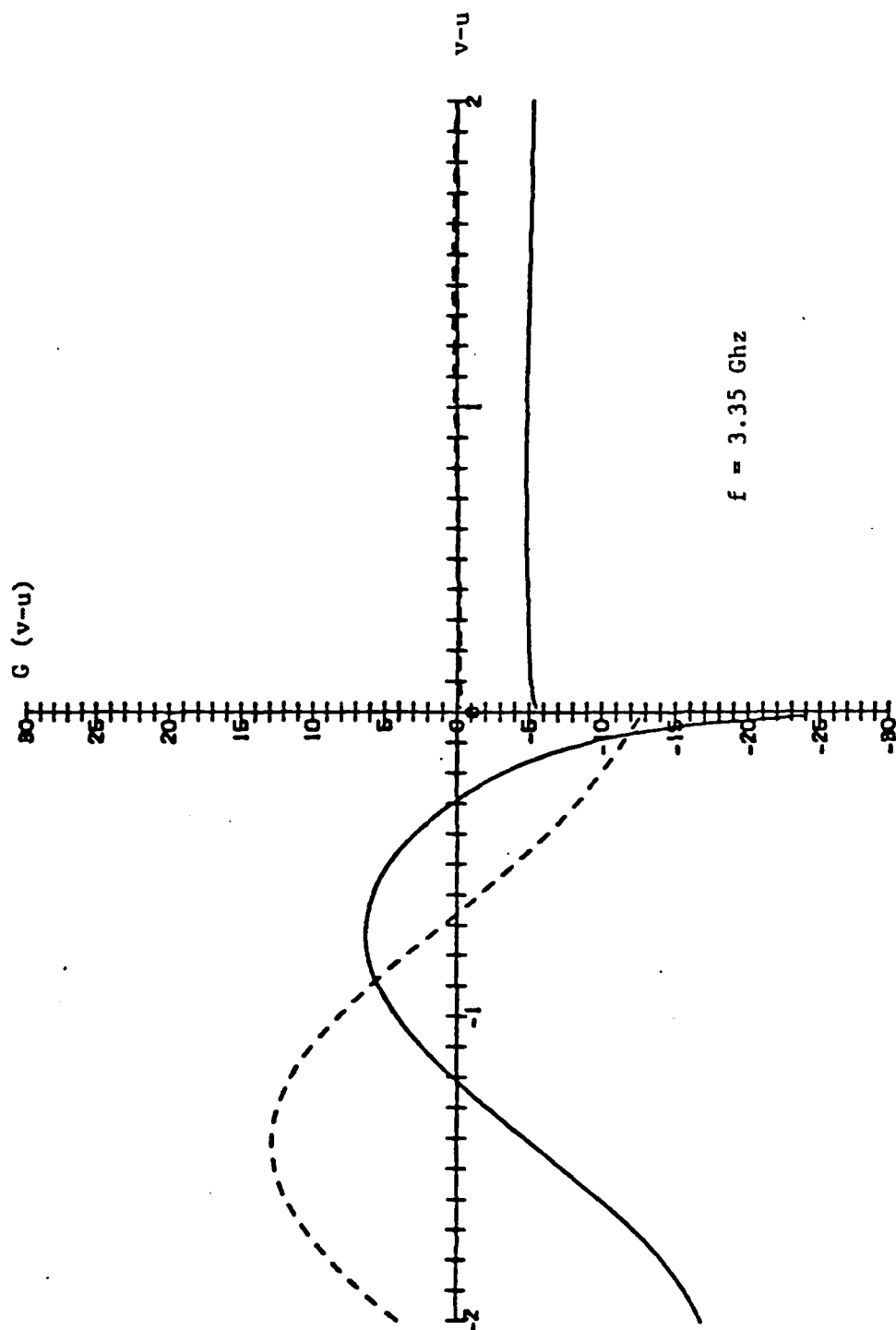


Fig. 2.19

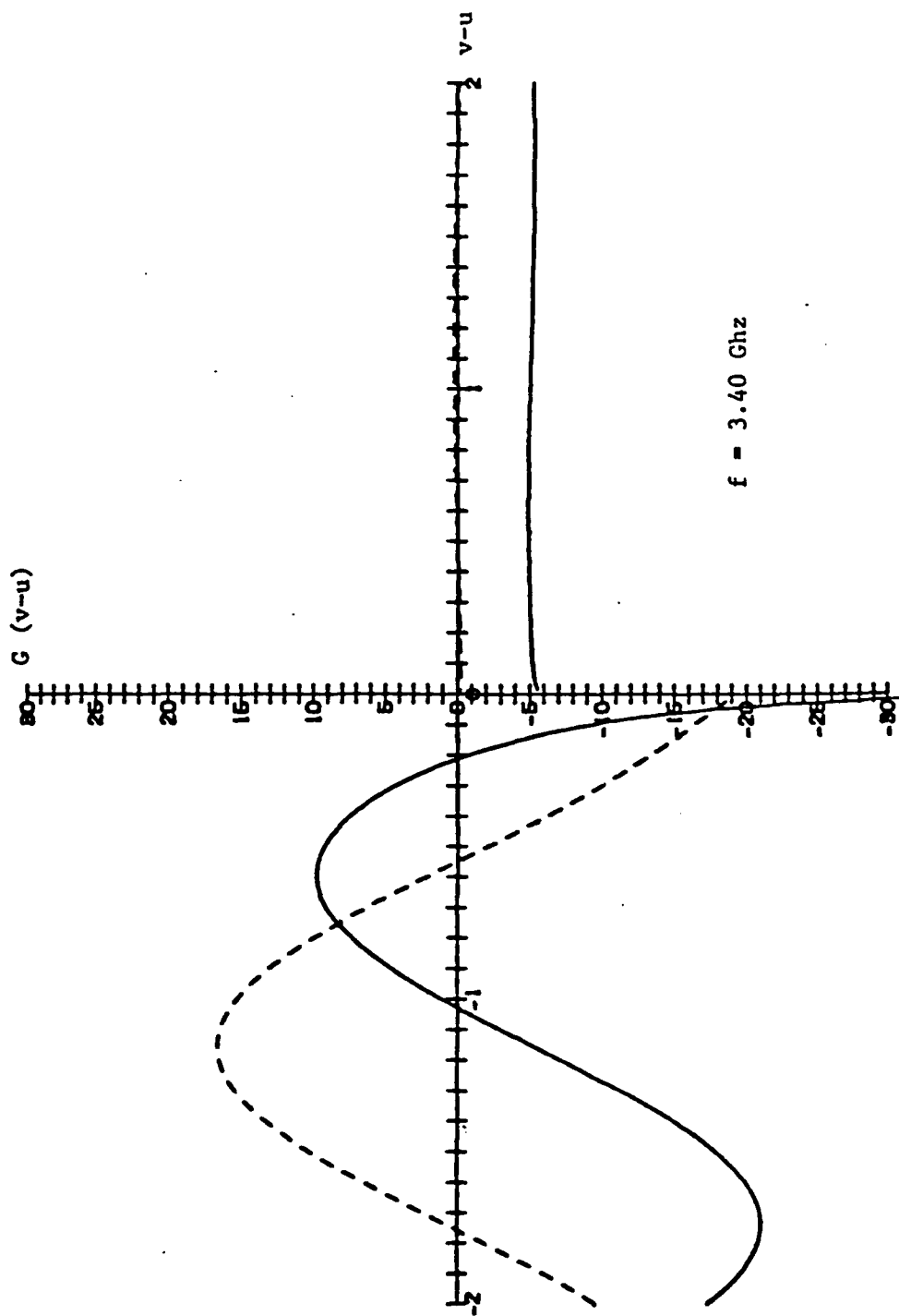


Fig. 2.20

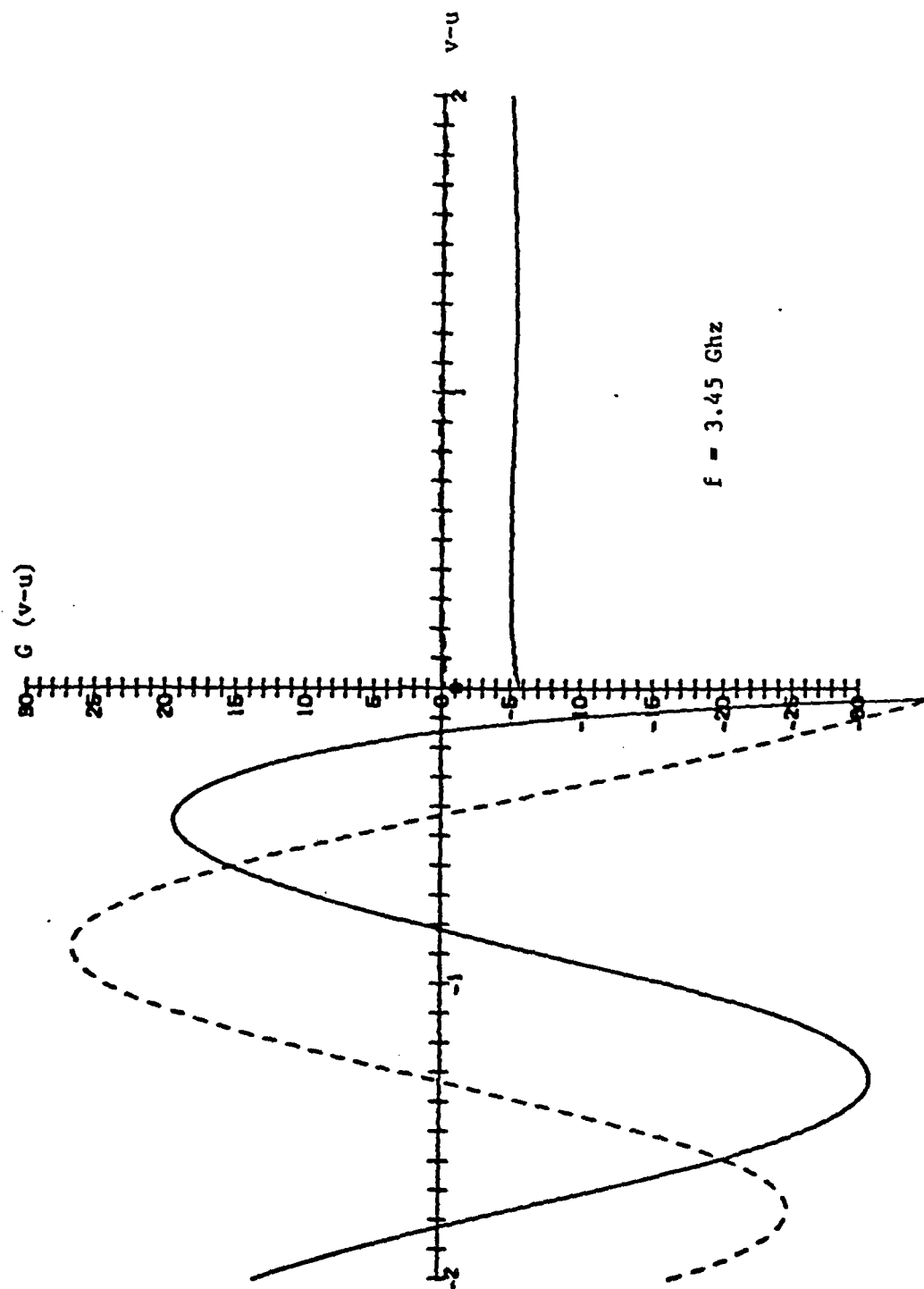


Fig. 2.21

REFERENCES

1. Weinberg, J. I., "Analysis and Computer Studies for Magnetostatic Surface Wave Transducers", RADC-TR-81-96 Interim Report, May 1981.
2. Sethares, J. C., and Cohen, E., "Current Distributions on Gratings and Meanderlines: with MSW Applications", IEEE Trans. on Magnetics, MAG-18, No. 6, Nov. 1982, pp. 1613-1615.
3. Gerson, T. J., and Nadan, J. S., "Surface Electromagnetic Modes of a Ferrite Slab", IEEE Microwave Theory and Techniques, MTT-22, No. 8, August 1974, pp. 757-763.
4. Abramowitz, M., and Stegun, I. A., Handbook of Mathematical Functions, etc., National Bureau of Standards, Applied Mathematics Series 55, June 1964, pp. 228, 229.
5. Lighthill, M. J., Fourier Analysis and Generalized Functions, Cambridge University Press, p. 43.
6. Johnson, W. A., and Dudley, D. G., "Real Axis Integration of Sommerfeld Integrals: Source and Observation Points in Air", J. Radio Science, Vol. 18, No. 2, pp. 175-186, March-April 1983.
7. Mosig, J. R., and Gardiol, F. E., "Analytical and Numerical Techniques in the Green's Function Treatment of Microstrip Antennas and Scatters", IEEE Proc., Vol. 130, Pt. H, No. 2, March 1983, pp. 175-182.
8. Proceedings of the 1981 RADC Microwave Magnetics Technology Workshop, June 10 - 11, 1981, RADC-TR-83-15.
9. Hamming, R. W., Numerical Methods for Scientists and Engineers, McGraw-Hill, p. 205.
10. Broeck, J. V. and Schwartz, L. W., "A One Parameter Family of Sequence Transformations", SIAM J. MATH. ANAL., Vol. 10, No. 3, May 1979, pp. 658-666.

3. MODESEARCH and FASTMC Program Conversions and Implementations

MODESEARCH and FASTMC are a tandem set of computer programs written in the UNIVAC version of ASCII FORTRAN. ARCON successfully converted these programs for use on the CDC 6600 computer. A full description of the programs, including the theoretical background, may be found in References [1,2].

The MODESEARCH program is guided by control cards which allow the user to specify ionospheric profiles and ionospheric collision frequency profiles. The FORTRAN NAMELIST definition is used to enter other specifications, e.g., the geomagnetic field, the ground conditions, the distance of this slab from the transmitter. [See Appendix I]

Various output options are available. The FASTMC-compatible output is a card image file, in which the first card identifies the slab conditions. It is followed by the mode constants, two cards per mode, ending with a blank card. Appendix I illustrates a typical stream of control code, input data and output data.

FASTMC implements a mode-summing technique which calculates field strength at user-specified transmitter and receiver altitudes. [See Appendix II for control cards and sample input/output data]. Output options include the vertical and horizontal components of the amplitude and the corresponding distance from the transmitter, the results of which may be printed or plotted. In this instance, plots were obtained by using the TEKTRONIX Graphics Terminal (off-line mode) and its Hard Copy unit. [See Appendix III for examples of plots].

APPENDIX I

```

<TOP OF FILE>
HOLST,T300,CM120000.
ATTACH,XX,MODESEARCH,ID=HOLST.
FTNS(I=XX,L=0)
REQUEST,TAPE1,*PF.
L60.
CATALOG,TAPE1,MODESEARCHOUTPUT,ID=HOLST,MR=1.
RETURN,XX,L60,TAPE1.
EOR
NAME
  IDATUM
  AZIM=283.0, CODIP=21.0, MAGFLD=5.44E-5,
  EPSR=10.0, SIGMA=10.0E-3,
  BETA=0.5, SCLHTS=6.0, ENMIN=0.1, HPRIME=87.0,
  FREQ=23.0, RHO=0.0, REFLHT=50.0,
  RANGER=70.0,87.0, RANGE1=0.0,-1.0,
  IEND
QUIT
<BOTTOM OF FILE>

```

3334 HOLST

```

<TOP OF FILE>
R 0.000 F 23.0000 A 283.000 C 21.000 M .544E-04 S 1.000E-02 E 10.0 T 87.0
1 89.91283 -6.502712-3.33252104E-05-2.37283889E-04-1.29396032E-09-1.55444857E-10
2 89.91283 -6.502712-4.13669031E-07-3.78898638E-07 9.90072854E-01 6.71432292E-02
1 89.74584 -5.505621 5.50719615E-04-4.78805072E-03-6.42842801E-10-5.42580297E-11
2 89.74584 -5.505621 1.16720717E-06 1.33227612E-06 9.88844736E-01 6.61828827E-02
1 87.88375 -.913771-5.32683379E-03-2.30771489E-02-4.32628737E-09-3.35977677E-09
2 87.88375 -.913771-6.48275418E-06-9.45516889E-06 9.85049639E-01 6.38126194E-02
1 85.91200 -.370342 4.24848636E-03-8.75920738E-03-2.23193224E-08 2.38319225E-09
2 85.91200 -.370342 8.94973443E-06 1.19011255E-05 9.83474238E-01 6.30287850E-02
1 81.32110 -.445981-5.68746234E-03-1.91768894E-02-2.37875909E-08-1.73385229E-08
2 81.32110 -.445981-1.47369354E-05-1.96120402E-05 9.76634392E-01 5.82415272E-02
1 80.10598 -.303952 5.81933423E-03-9.44696655E-03-6.33511608E-08 1.60567308E-08
2 80.10598 -.303952 1.67737623E-05 2.14987653E-05 9.73579686E-01 5.67294411E-02
1 76.27959 -.359672-7.38935438E-03-1.01423447E-02-1.01074771E-07-5.39628050E-08
2 76.27959 -.359672-2.97935702E-05-2.46164902E-05 9.61396854E-01 4.85706901E-02
1 75.23709 -.451541 7.98421382E-03-1.59733251E-02-7.39162419E-08 5.26071924E-08
2 75.23709 -.451541 3.18594953E-05 2.59897420E-05 9.57316804E-01 4.52404947E-02
1 71.59467 -.281662-5.24635889E-03-3.32464239E-03-2.50195109E-07-6.83767739E-08
2 71.59467 -.281662-3.61979008E-05-1.60890849E-05 9.37180159E-01 3.21704217E-02

<BOTTOM OF FILE>

```

APPENDIX II

```
EDIT.  
P$  
<TOP OF FILE>  
HOLST,CH100000,T100. 3334 HOLST  
ATTACH,XX,FASTMC,ID=HOLST.  
FIN5(I=XX,L=0)  
ATTACH,TEK,TEKOFFLINE.  
LIBRARY(TEK)  
ATTACH,TAPES,FASTMCDATA,ID=HOLST.  
REQUEST,T40140,*PF.  
L60.  
CATALOG,T40140,FASTMCPLLOT,ID=HOLST.  
RETURN,TAPES.  
RETURN,XX,L60.  
<BOTTOM OF FILE>
```

APPENDIX II (continued)

<TOP OF FILE>

NAME

SDATUM

NPRINT=1, ICOMP=1, NRCURV=2,

TALT=0.0, RALT=0.0,

AMPMIN=-.7E+02, SIZEY=7.0,

SEND

DATA

FASTMC TEST RUN

R 0.000 F 23.0000 A 203.000 C 21.000 M .544E-04 S 1.000E-02 E 10.0 T 87.0
1 89.91283 -6.502712-3.33252104E-05-2.37283889E-04-1.29396032E-09-1.55444857E-10
2 89.91283 -6.502712-4.13669031E-07-3.78898638E-07 9.90072054E-01 6.71432292E-02
1 89.74584 -5.505621 5.50719615E-04-4.78805072E-03-6.42042001E-10-5.42580297E-11
2 89.74584 -5.505621 1.16720717E-06 1.33227612E-06 9.88844736E-01 6.61828827E-02
1 87.88375 -.913771-5.32683379E-03-2.30771489E-02-4.32628737E-09-3.35977677E-09
2 87.88375 -.913771-6.48275418E-06-9.45516889E-06 9.85049639E-01 6.38126194E-02
1 85.91200 -.370342 4.24848636E-03-8.75920738E-03-2.23193224E-08 2.38319225E-09
2 85.91200 -.370342 8.94973443E-06 1.19011255E-05 9.83474238E-01 6.30287850E-02
1 81.32110 -.445981-5.68746234E-03-1.91768894E-02-2.37075909E-08-1.73385229E-08
2 81.32110 -.445981-1.47369354E-05-1.96120402E-05 9.76634392E-01 5.82415272E-02
1 80.10598 -.303952 5.81933423E-03-9.44696655E-03-6.33511608E-08 1.60567308E-08
2 80.10598 -.303952 1.67737623E-05 2.14987653E-05 9.73579686E-01 5.67294411E-02
1 76.27959 -.359672-7.38935438E-03-1.01423447E-02-1.01074771E-07-5.39626050E-08
2 76.27959 -.359672-2.97935702E-05-2.46164902E-05 9.61396854E-01 4.85706901E-02
1 75.23709 -.451541 7.98421382E-03-1.59733251E-02-7.39162419E-08 5.26071924E-08
2 75.23709 -.451541 3.18594953E-05 2.59897420E-05 9.57316904E-01 4.52404947E-02
1 71.59467 -.281662-5.24635889E-03-3.32464239E-03-2.50195109E-07-6.03767739E-08
2 71.59467 -.281662-3.81979008E-05-1.60090849E-05 9.37100159E-01 3.21704217E-02

R 3.000 F 23.0000 A 203.000 C 21.000 M .544E-04 S 1.000E-02 E 10.0 T 87.0

R 7.000 F 23.0000 A 203.000 C 21.000 M .544E-04 S 1.000E-02 E 10.0 T 87.0

R 40.

NAME

SDATUM

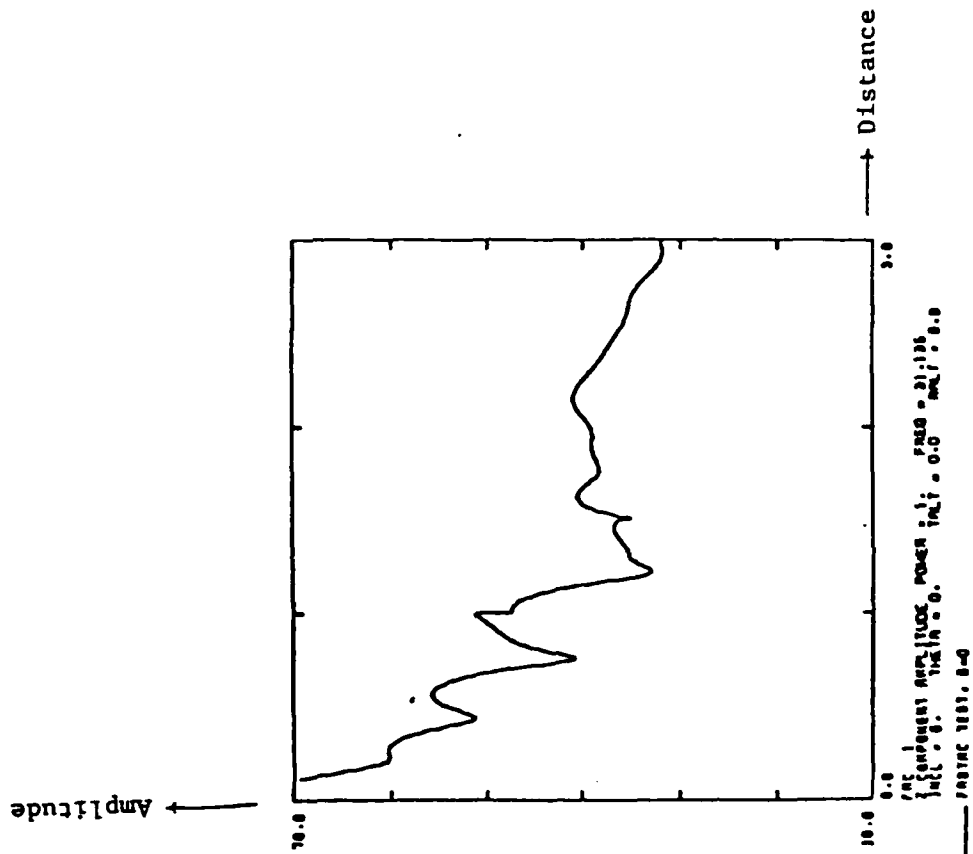
ICOMP=2,

SEND

START

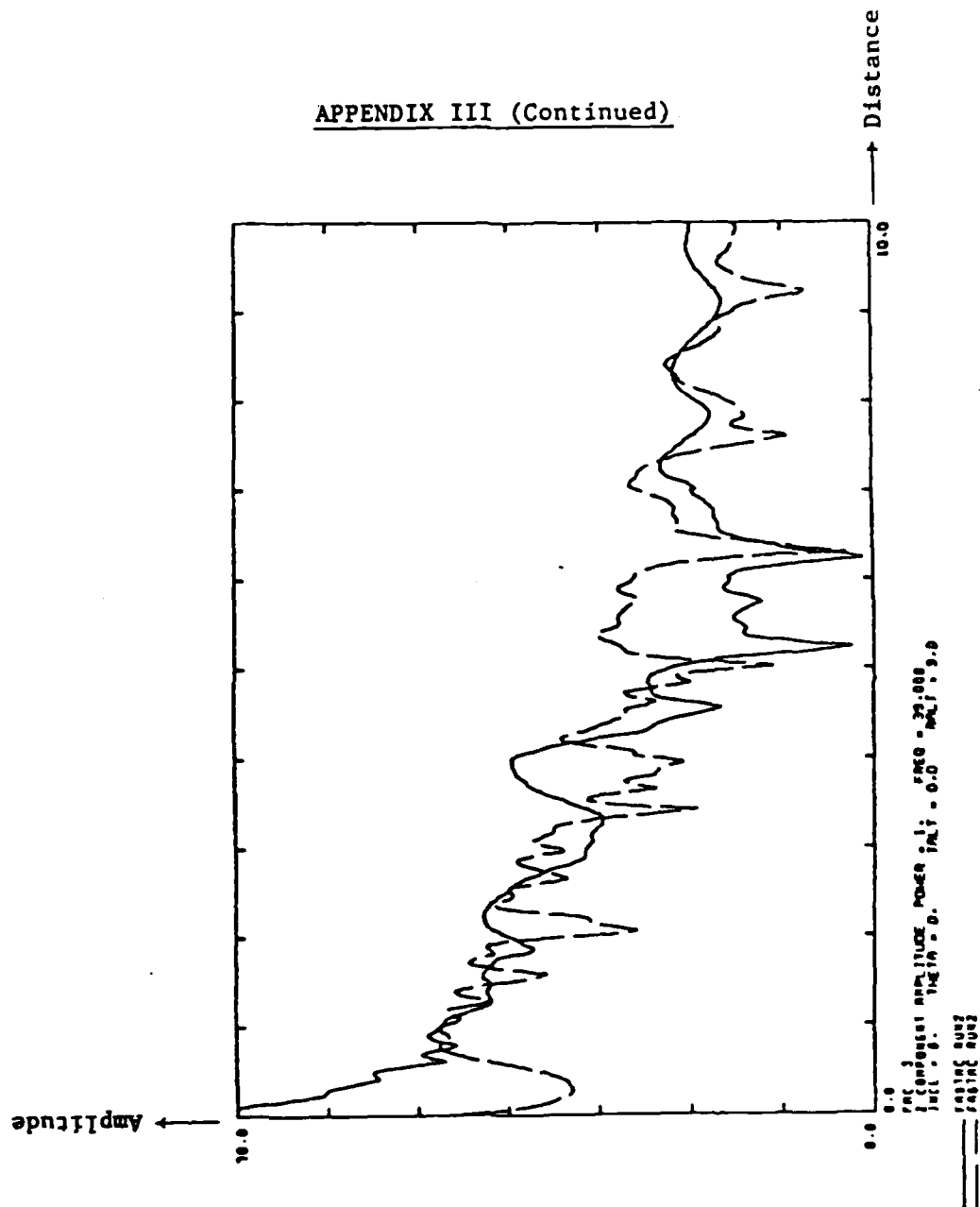
<BOTTOM OF FILE>

APPENDIX III



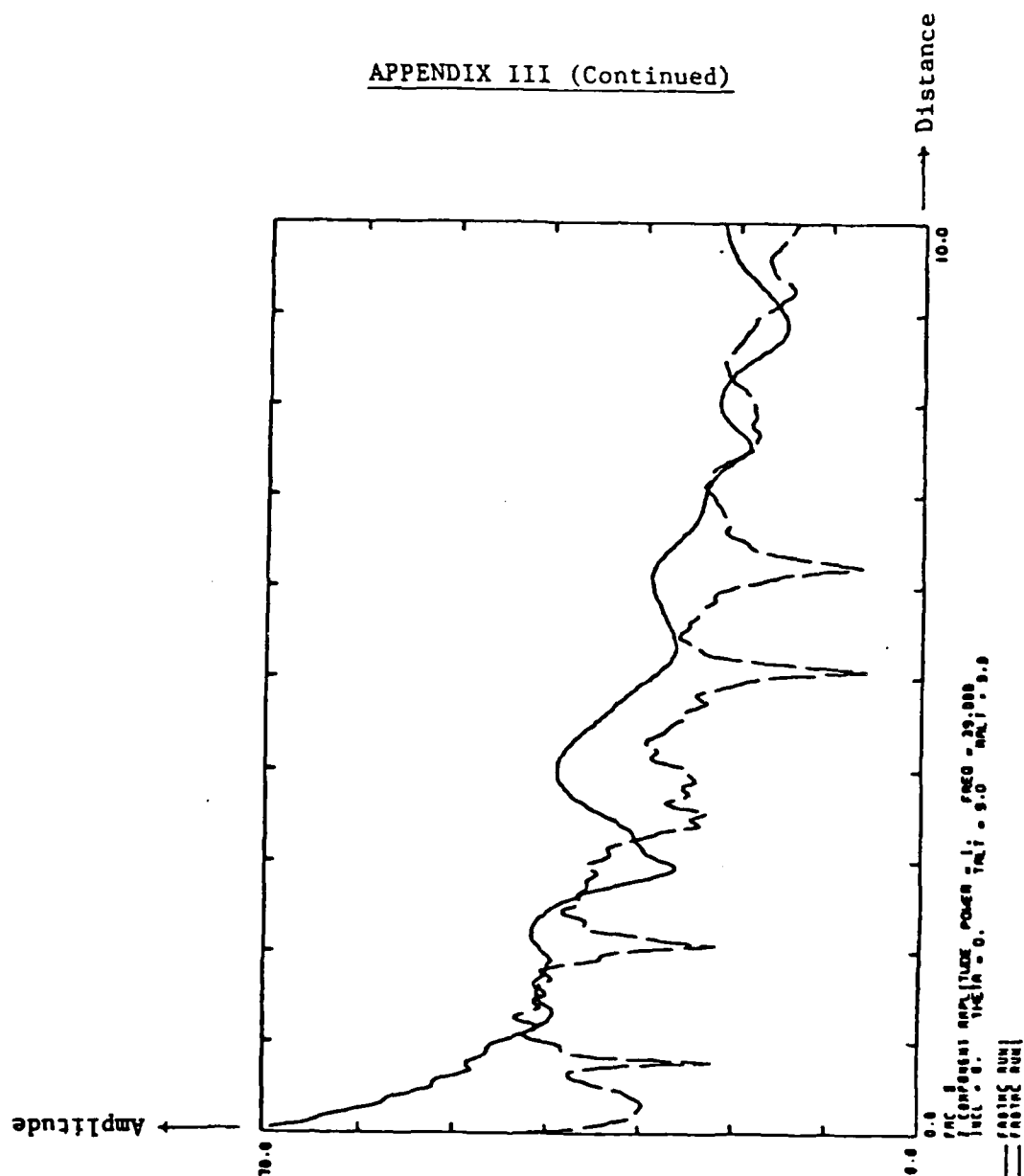
91-22-00 00/12/00 2

APPENDIX III (Continued)



2 00/10/07 09:55:12

APPENDIX III (Continued)



85-65-11 CB/01/90 7

REFERENCES

1. D. G. Morfitt and C. H. Shellman, MODESRCH, An Improved computer Program for Obtaining ELF/VLF/LF Mode Constants in an Earth-Ionosphere Waveguide, Defense Nuclear Agency Interim Report 77T, 1 October 1976.
2. J. A. Ferguson and F. P. Snyder, Approximate VLF/LF Waveguide Mode Conversion Model, Computer Applications: FASTMC and BUMP, Naval Ocean Systems Center Technical Document 400, 18 November 1980.

4. OTH Radar Data Analysis

4.1 Introduction

The Over-the-Horizon Experimental Radar System (ERS) operated from June 1980 to June 1981. Data from this period was made available in compressed form on magnetic tapes. ARCON was requested to provide programming support for the analysis of the data.

The purpose of this effort was to make recommendations for improving the assessment of clutter by studying the clutter behavior. A detailed presentation of the background and design of the analysis, with results of the initial phase, and proposal for further work, may be found in an in-house report [Ref. 1].

The discussion below will focus on the programming effort, in particular on four programs. Each program comprises a tandem set of subprograms, the first of which performs the required data sort. The remainder provide options for presenting the data sort in printed displays.

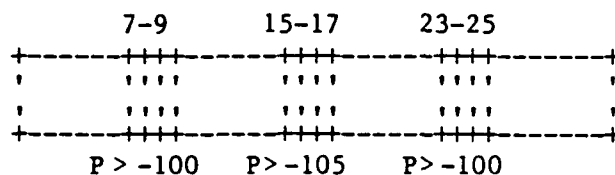
1. POWERLEVEL/POWERDISPLAY
2. BINSORT/BINDISPLAY
3. SPEEDSORT/SPEEDDISPLAY
4. SPREADSORT/SPREADDISPLAY

The summary data is stored in unformatted (binary) form on magnetic tapes, separately by season. Each data record contains a header with information such as date and time, transmitter power, operating frequency, wave repetition frequency, and range-azimuth values. The corresponding range-azimuth array follows, in which the 32 cells for each combination represent the doppler-shifted power return to the radar.

Figure 4-1 shows a sample record. Note that the actual ERS array element is the negative of the printed element.

4.2 Program POWERLEVEL

For each spectrum, the program POWERLEVEL counts the occurrence of power above a specified value for each range-azimuth element in three doppler bin groups. The counts are separated further by operating frequency, Kp value, and time of day.



The counts are separated according to

Azimuth	(7 levels):	10 to 80 deg
Range	(8 levels):	1380 to 3000 km
Bin group	(3 levels):	7-9, 15-17, 23-25
Kp value	(3 levels):	0-6, 7-15, 16-27
Frequency	(3 levels):	6-11, 12-16, 17-21 Mhz
Time	(3 levels):	0-8, 8-16, 16-24 UT

The sorted data is saved in a permanent file. POWERDISPLAY reads this file and prints range-azimuth arrays for combinations of doppler group, Kp value, frequency, and time of day. Each printed element includes the number of counts made and the number of findings of power above the specified level. Another display option provides data counts combined over all Kp values, all frequencies, etc.

Figure 4-2 shows a diagram.

4.3 Program BINSORT

For each spectrum, the program BINSORT applies a filter to the ground clutter level (bins 15-17). A count is made of the number of occurrences of average power greater than a specified value. This count is placed in the category Looks, separated by azimuth, range, and time (24 levels, each 1 hour).

If the filter condition is satisfied, then the doppler shifted power average is computed for bins 7-9 and bins 23-25, respectively. This sample is placed in one of the categories

1. Approach
2. Recede
3. Flat

(or counted as "other") based on a comparison of the power averages.

Figure 4.3 shows a diagram.

Filter and sort levels, as well as the power difference are inputs to the program.

The sorted data is saved in a permanent disk file. A set of DISPLAY programs prints the data counts in range-azimuth arrays for each category (Approach, Recede, Flat). Each array element includes the number of Looks and the number of findings for the category.

The range-azimuth arrays of data counts may be printed for 1-hour time intervals or for 24 hours combined. In addition, the arrays may be printed for 4-hour time groups, shifted by 1-hour increments:

Time Group	1:	0000-0400 UT
	2:	0100-0500
	23:	2200-0200
	24:	2300-0300

Another variation provides the number of "hits" of Approach, Recede and Flat in percent relative to the total number of Looks. The 4-hour time groups are used, as above, but with no separation into range-azimuth arrays.

4.4 Program SPEEDSORT

The program SPEEDSORT implements a formula for associating each bin with a speed value, as follows:

$$v = - VMAX \times A \quad [m/s]$$

(1)

where

$$V_{MAX} = (WRF/4) \times (c/f_{op}) \quad (2)$$

WRF = wave repetition frequency (Hz)

f_{op} = operating frequency (Hz)

c = velocity of light = 3×10^8 m/s

and

$$A = [K_o - 2(K-1)]/K_o \quad (3)$$

K_o = number of bins = 32

K = bin number (1-32)

so that $K = 1, 2, \dots, 16, 17, 18, \dots, 32$

yields $A = 1, +.937, \dots, +.0625, 0, -.0625, \dots, -.937$

[Note: currently, bin 1 is omitted to provide symmetry.]

This calculation is performed for each data record. A search is then made for speed values within a specified interval [e.g., (-125 to -75) or (75 to 125)]. The corresponding bin numbers, if any, are retained.

For each spectrum, a filter is applied to the power in bin 17. A count is made of the number of occurrences of power greater than a specified value. This count is placed in the category Looks, separated by azimuth, range, and time (24 levels, each 1 hour). If the filter condition is satisfied, then the doppler-shifter power average is computed. The bins are selected according to their corresponding speed value.

This sample is placed in one of the categories

1. Approach
2. Recede
3. Flat

or counted as "other" based on comparison of the power averages (as in BINSORT).

The sorted data is saved in a permanent disk file. Display options are the same as for BINSORT.

The speed interval is an input to the program along with the filter and sort levels, as well as the power difference.

4.5 Program SPREADSORT

The program SPREADSORT calculates the difference between the power in bin 17 and the average power over bin groups corresponding to a specified speed interval. That is, no filter is applied at the ground clutter level or the doppler-shifted level. The placement of spectra into categories is determined by the spread between these levels. The bin groups are selected according to the speed formula described for SPEEDSORT. A count is made for occurrences of differences greater than a specified quantity (e.g., 40 dBw). This sample is placed in a category as follows:

1. Double - if the condition is satisfied on both sides of the spectrum
2. Approach - if the condition is satisfied on the left side of the spectrum
3. Recede - if the condition is satisfied on the right side of the spectrum

Display options are the same as for BINSORT and SPEEDSORT.

The speed interval and power difference are inputs to the program.

1 1980 DAY 224 TIME 31 TRANSMITTER POWER = 58.46 FREQUENCY = 18.25 UHF = 45.00
 AZ = 31.55 36.55 41.55 46.55 51.55 56.55 61.55
 RS = 2400.0 2600.0 2800.0 3000.0

101	99	106	109	108	110	111	112	112	111	112	112	111	112	107	104	98	98	79	65	65	83	100	111	112	113	114	112	114	115	113	112	110	106	106	
102	103	104	103	102	102	100	106	107	104	105	104	105	105	104	105	105	103	73	68	66	77	92	100	103	104	105	104	104	108	105	105	103	105	102	
103	103	102	102	104	106	102	103	104	104	105	105	105	104	104	104	104	99	84	76	78	88	94	103	105	106	108	110	106	104	105	104	101	103	103	
113	112	109	110	111	114	114	113	112	111	112	110	109	110	101	101	101	85	82	90	94	95	102	105	113	116	116	119	115	114	115	113	112	111	111	
127	125	130	135	134	132	133	134	132	120	122	126	121	116	110	79	62	63	86	115	123	126	128	127	130	131	133	131	132	126	122	120	122	122	122	
126	126	124	125	123	123	126	126	124	123	123	123	117	117	105	74	63	67	87	105	109	114	118	122	125	125	128	126	126	122	120	122	122	122	122	
107	109	111	109	109	108	109	111	112	112	114	114	113	113	104	74	63	67	93	101	108	112	115	114	113	112	112	113	113	112	111	111	112	112	112	
113	112	114	115	112	114	114	114	114	114	114	114	112	111	110	112	104	85	77	85	102	106	110	116	116	115	117	118	118	117	110	119	114	113	113	
127	125	127	128	125	124	128	124	122	122	123	122	121	116	115	82	64	64	89	114	112	116	121	124	129	128	129	129	129	129	126	128	129	129	129	129
135	140	138	137	137	135	135	139	135	131	126	128	125	122	115	84	63	64	89	123	123	125	127	127	134	136	134	133	134	133	134	133	135	134	134	
129	133	133	131	133	132	131	133	132	130	127	124	124	127	119	82	65	67	94	112	115	115	113	118	124	130	130	124	129	129	129	129	129	129	130	
130	129	129	128	129	128	131	129	129	127	123	122	122	119	117	82	71	73	99	116	113	115	126	127	128	131	133	136	133	135	135	135	135	135	135	
132	132	130	134	132	132	132	132	133	126	125	126	123	115	111	71	62	68	99	109	115	123	124	123	131	135	135	133	133	131	133	131	133	133	133	
137	139	138	137	138	136	138	138	136	130	125	125	124	122	114	78	67	71	98	125	127	120	129	127	132	134	137	135	135	137	135	137	132	129	129	
136	136	134	136	136	135	136	133	134	130	128	127	126	122	117	81	70	72	100	114	116	120	121	124	130	129	128	120	131	134	134	134	134	134	133	
135	138	137	137	140	141	138	137	137	132	130	130	126	126	117	84	74	78	195	120	120	119	123	128	136	135	135	135	135	137	135	137	137	137	136	
135	136	138	138	136	134	135	134	131	121	122	124	121	119	103	64	59	72	107	110	115	121	124	127	133	132	132	132	134	139	136	121	120	120		
137	136	136	136	137	134	136	139	136	129	126	126	119	115	114	78	65	68	99	121	126	125	127	127	130	132	132	134	134	134	134	136	136	136	136	
136	136	137	137	139	136	138	136	133	133	128	125	121	124	115	80	70	73	102	116	119	120	122	122	127	131	134	134	134	134	134	136	136	137	137	
139	138	135	136	137	134	134	134	130	125	125	126	121	121	119	86	70	72	100	108	111	116	122	126	133	135	135	137	138	136	136	136	136	135	135	
135	136	138	138	135	132	134	134	131	121	126	127	120	117	103	64	56	70	103	119	120	118	118	126	132	132	132	132	132	132	136	133	133	134	134	
138	135	135	137	136	133	136	136	131	122	127	128	127	123	103	63	57	71	104	117	122	129	125	128	134	135	135	135	135	135	140	128	133	134	134	
134	133	134	134	136	132	133	134	137	128	125	128	122	122	113	80	64	67	82	117	120	123	120	116	119	126	129	131	134	133	133	133	135	135	135	
139	134	132	136	137	136	137	133	137	133	127	130	127	122	122	85	69	68	87	120	123	123	126	131	132	133	133	133	132	137	133	133	133	136	136	
134	136	136	136	135	136	135	132	132	126	128	128	121	114	107	67	60	73	104	117	117	120	121	124	127	131	134	132	132	132	134	133	133	136	136	
131	131	131	130	132	132	128	127	123	120	121	119	116	115	102	64	59	72	86	112	115	117	121	127	130	132	133	130	131	134	133	133	133	133	133	
138	139	137	135	137	132	130	132	131	127	126	125	117	112	106	75	68	75	91	110	121	122	123	122	124	128	134	134	132	135	135	135	135	135	135	
136	137	135	136	134	137	134	131	134	127	124	122	121	120	115	88	76	79	99	121	123	121	121	123	125	132	134	130	133	135	135	135	135	134	134	

Fig. 4-1

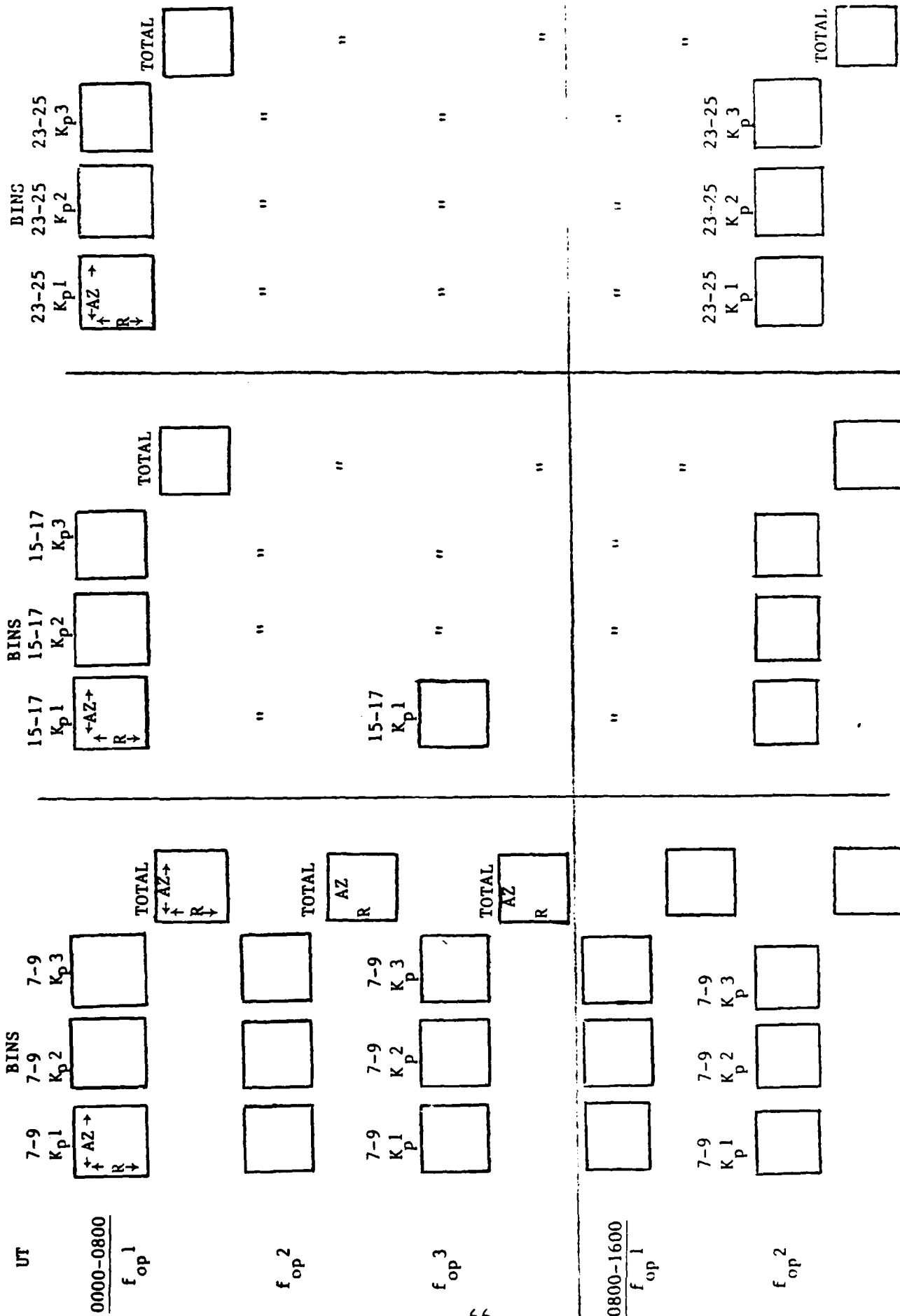


Fig. 4-2

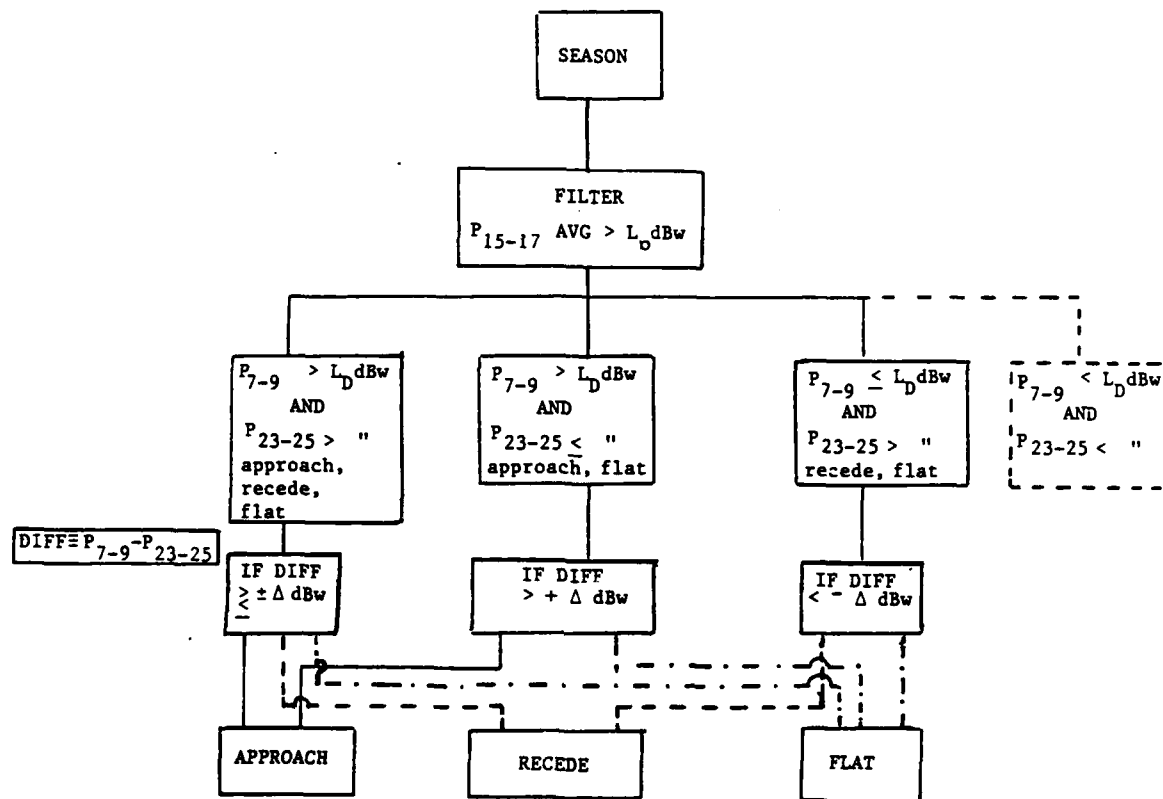


Fig. 4-3

REFERENCES

1. Toman, K., Experimental Radar System Auroral Clutter Statistics, RADC/EEPI, (to be published).

5. Meteor Scatter Model

ARCON was requested to provide programming support to demonstrate the operation of an experimental meteor-scatter model. An outline of the basic computation flow follows:

- I. Determine, from the geographic location of the stations, the quantities f and a . (For Thule-Sondrestrom, $f = 600$ km, $a = 6400$ km.) $h_l = 80$, $h_u = 120$.
- II. Choose a direction of meteorite flow,
 $\theta = 135^\circ$, $\phi = 45^\circ$.
- III. Produce a series of "b-sheets", one for each value of b (for testing, $b = 130$ to 400 , in 10 km steps).
- IV. For a given b , x varies in the interval:
 $-b \leq x \leq b$ [1 km steps].

Calculate quantities: y , z , u , v .

$$y = \frac{-ABx + \sqrt{(ABx)^2 - CD}}{C} \quad (1)$$

$$A = \sin\theta \cos\phi \quad (2)$$

$$B = \frac{b^2}{b^2 + f^2} \sin\theta \sin\phi \quad (3)$$

$$C = \frac{b^2}{b^2 + f^2} \left(\frac{b^2}{b^2 + f^2} \sin^2\theta \sin^2\phi + \cos^2\theta \right) \quad (4)$$

$$D = (\sin^2\theta \cos^2\phi + \cos^2\theta) x^2 - b^2 \cos^2\theta \quad (5)$$

$$z = \sqrt{b^2 - \frac{b^2}{b^2 + f^2} y^2 - x^2} \quad (6)$$

$$u = x \sin\phi - y \cos\phi \quad (7)$$

$$v = -x \cos\theta \cos\phi - y \cos\theta \sin\phi + z \sin\theta \quad (8)$$

Calculate restrictions.

$$\text{Tangent Plane @ R} \quad z \geq \frac{f}{\sqrt{a^2 - f^2}} (f-y) \quad (9)$$

$$\text{Tangent Plane @ T} \quad z \geq \frac{f}{\sqrt{a^2 - f^2}} (f+y) \quad (10)$$

$$\text{Lower Zone - Boundary} \quad z \geq \sqrt{(a - h_l)^2 - (x^2 + y^2)} - \sqrt{a^2 - f^2} \quad (11)$$

$$\text{Upper Zone - Boundary} \quad z \geq \sqrt{(a + h_u)^2 - (x^2 + y^2)} - \sqrt{a^2 - f^2} \quad (12)$$

V. Plot a restricted hot-line u vs. v for each value of b .

VI. The extrema of the restricted hot-lines define an area ("cross-section") in u - v space. Measure this area in square km, and tabulate vs θ, ϕ .

VII. Repeat, starting at II, using a new meteorite direction θ, ϕ .

The programming effort has progressed through Step V. Printed output was obtained for each b value.

A plotting structure provides various options:

1. Plot u, v corresponding to z values that satisfy the given restrictions.
2. Plot all u, v ; use special symbol to indicate those in restricted area.
3. Plot x, y ; use special symbol to indicate those corresponding to restricted u, v .

The TEKTRONIX Graphics Terminal and its Hard Copy unit were used for plot output. Examples of the plotted output are shown in Fig. 5-1 - 5-3.

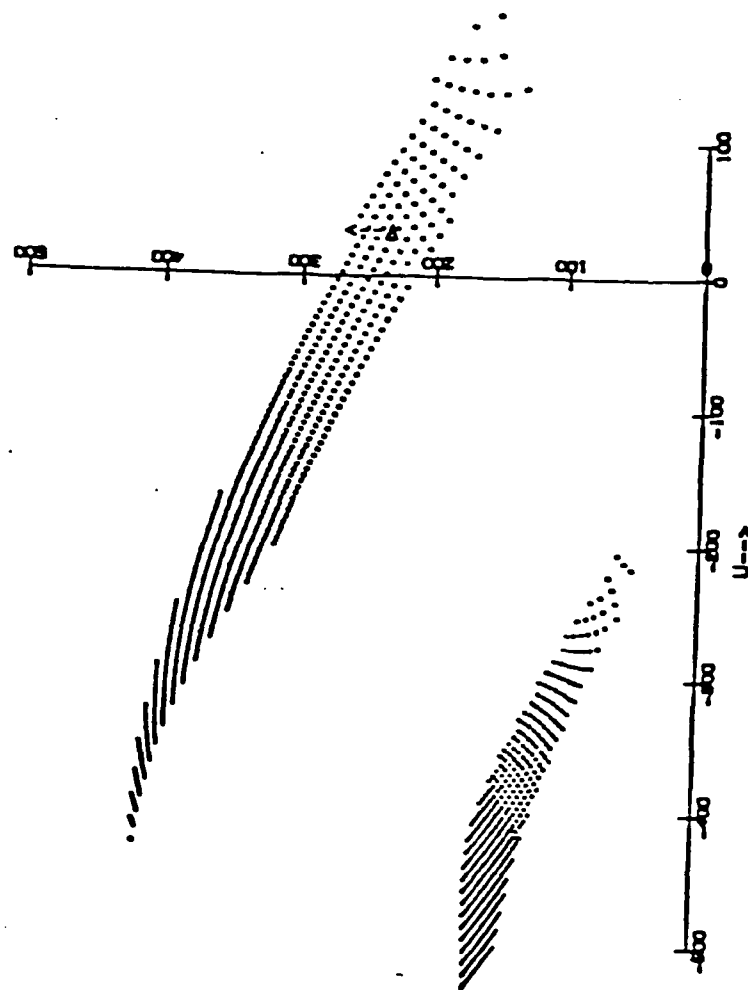


Fig. 5-1

Good u, v
 $b = 130, 400$
 $hinc = 10$

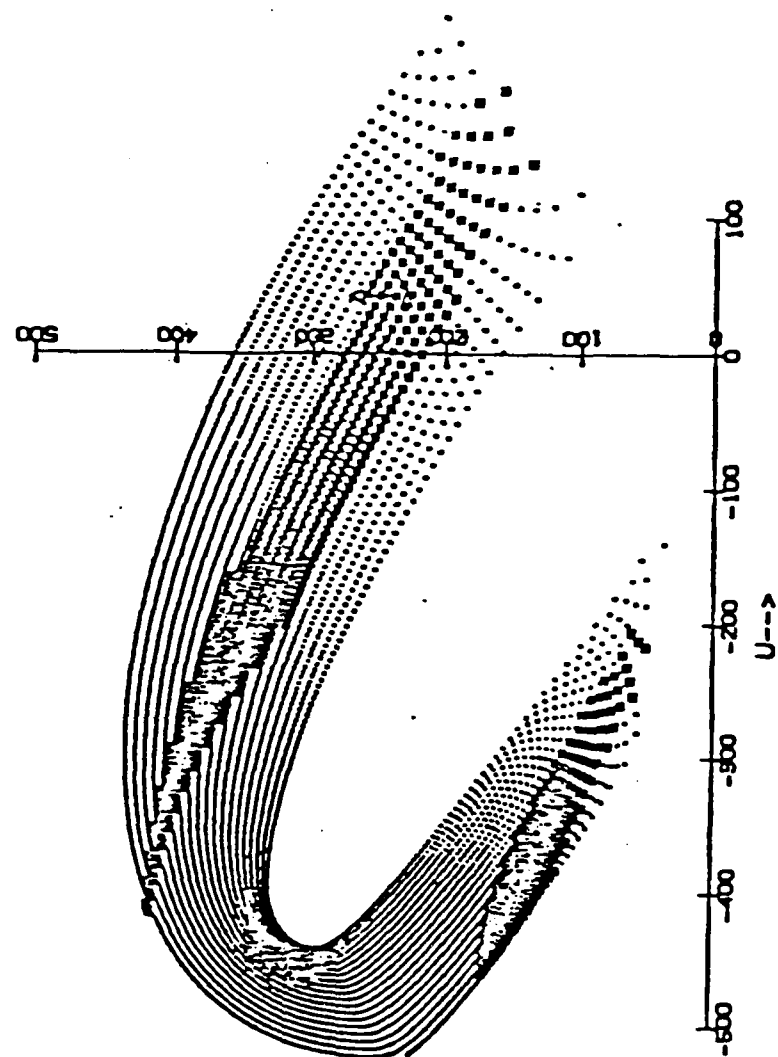


Fig. 5-2

ALL u,v
b = 130, 310+
binc = 10

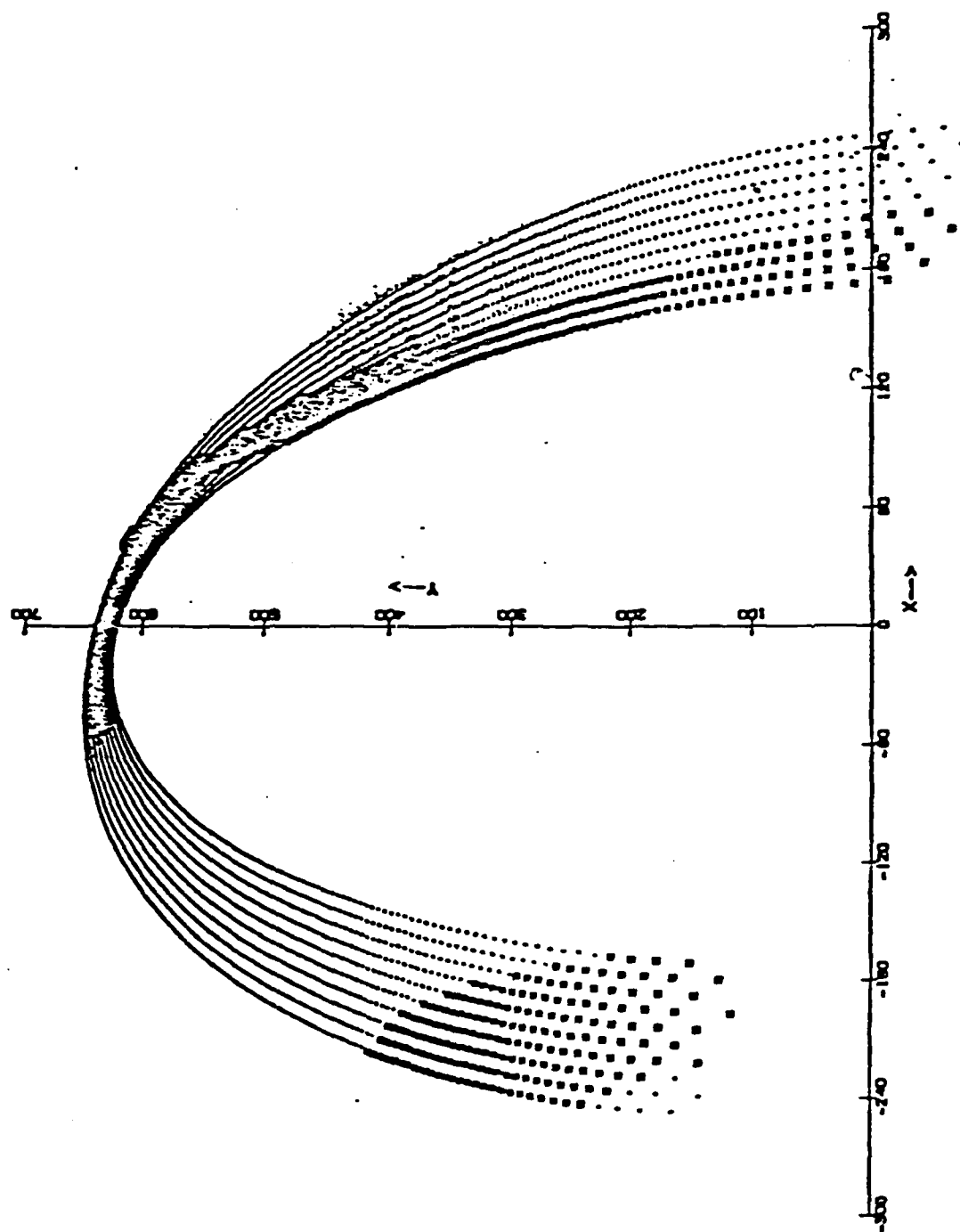


Fig. 5-3

6. Direct and Multipath Communications Data Analysis

6.1 Introduction

The task was to provide software support for reading, processing, and plotting communications data representing signal amplitude as a function of several variables. In particular the work centered about the investigation of the following dependencies:

- (a) amplitude as a function of atmosphere conditions;
- (b) amplitude as a function of the transmitting antenna's elevation;
- (c) amplitude as a function of the time between the initial signal transmission and corresponding signal reception.

Data was studied as a function of two variables by combining dependence (a) with dependence (b) or (c). The first combination is known as angle-of-arrival data, or AOA data, and the second combination as time-of-arrival data, or TOA data.

The data were invariably written on magnetic tapes with each tape containing approximately 24 hours of data, i.e., each tape was associated with data for exactly one day of the given year. Since for every day of the Gregorian calendar, one can find the Julian calendar day, we labeled the tapes using Julian dates. For example, tape BA2256 represents angle-of-arrival date for 1982, day #256, i.e., September 13. Letter B was used to indicate the data tape was a backup copy of the original tape.

6.2 Data Tape Content and Task Orientation

Each tape contained approximately 200 records, usually from 150 up to 220 records. Each record contained 64 signals, with each signal display referred to as a signal scan. The length of the scan - the number of points in the scan - was different: 64 for angle-of-arrival, and 192 for time-of-arrival data. The time interval between two sequential signals equaled 6 seconds.

The first main task was to produce perspective on (pseudo-) 3-dimensional plots. Because technical details such as length of axes, tickmarks, headers, labels and so on were different from AOA and TOA data, 2 sets of programs were prepared. Thus, program AOATHREED produced 3-dimensional plots for angle-of-arrival data, and program TOATHREED produced 3-dimensional plots for time-of-arrival data. These programs used logarithmically transformed data. We also prepared slightly modified programs, LINAOA and LINTOA, in order to accommodate a request to use linear data. Detailed description of all control cards and input cards is given in Appendix A.

The next task was to perform cross-correlation analysis between angle-of-arrival data. Program ADACOR was constructed and consisted of two logically independent parts: the second part for making 3-dimensional plots, as usual, and the first part for performing cross-correlation analysis via Fast Fourier Transform technique (FFT).

In general, we used the second scan from the first record of the current tape as a standard signal and during the cross-correlation process all other scans from the same tape were compared with this standard signal. (Note: Of course, it would be even more natural to use the first scan as a standard signal, but the first scan was always defective.) We also had to provide for the case, when the second scan was not desired as a standard signal. So, program CORWRITE prepared a permanent file, containing a standard signal, and program CORREAD then used this standard signal for correlation purposes.

6.3 Correlation Analysis

The cross-correlation function of two sets of random data describes the general dependence of the values of one set of data on the other. Consider the pair of time history records $x(t)$ and $y(t)$. An estimate for the cross-correlation function of the values of $x(t)$ at time t and $y(t)$

at time $(t + \sigma)$ may be obtained by taking the average product of the two values over the observation time T . For stationary data, the resulting average product will approach an exact cross-correlation function as T approaches infinity. That is,

$$R_{xy}(\sigma) = \lim_{T \rightarrow \infty} \frac{1}{T} \int_0^T x(t)y(t+\sigma)dt. \quad (1)$$

If $R_{xy}(\sigma) = 0$, $x(t)$ and $y(t)$ are said to be uncorrelated. For a faster implementation of this process, we used the Fast Fourier Transform Technique instead of the direct (standard) method.

6.4 Fast Correlation

An infinite-range Fourier Transform of a real-valued or a complex-valued record $x(t)$ is defined by the complex-valued quantity

$$X(f) = \int_{-\infty}^{\infty} x(t) e^{-j2\pi ft} dt \quad (2)$$

Theoretically, this transform $X(f)$ will not exist for an $x(t)$ which is a representative member of a stationary random process when the infinite limits are used. However, by restricting the limits to a finite time interval of $x(t)$, say in the range $(0, T)$, then the finite-range Fourier Transform will exist as defined by

$$X(f, T) = \int_0^T x(t) e^{-j2\pi ft} dt \quad (3)$$

The discrete version of this equation is

$$X(f, T) = h \sum_{n=0}^{N-1} x_n \exp [-j2\pi f_n h] \quad (4)$$

The usual selection of discrete frequency values for the computation of $X(f,T)$ is

$$f_k = kf = \frac{k}{T} = \frac{k}{Nh} \quad , \quad k = 0, 1, \dots, N-1 . \quad (5)$$

Fast Fourier Transform (FFT) methods are designed to compute the quantities, X_k , and can also be used to compute the coefficients for a standard Fourier series.

Returning to cross-correlation functions, there are two approaches to the estimation of cross-correlation functions, namely, the direct approach and the FFT approach.

The procedure for the second case is briefly described below.

Let

$$R_{xy}(r,h) = \frac{1}{N-r} \sum_{n=1}^{N-2} x_n y_{n+r} \quad , \quad r = 0, 1, \dots, m . \quad (6)$$

(If $N \gg m$, it may be more convenient to divide by N instead of dividing by $N-r$.)

The initial sample size for both $x(t)$ and $y(t)$ is assumed to be $N=2^P$. Here, $x(t)$ is the standard time signal against which all others are to be cross-correlated; $y(t)$ is the time signal to be cross-correlated.

Two separate FFTs are involved in these computations; one for $x(t)$ and one for $y(t)$. We computed the product of the two transforms, then their inverse transform again using the FFT procedure. It yielded an unnormalized cross-correlation, and the normalization was tailored to the initiator's needs.

In summary, we operated with 3 sets of 3-dimensional programs. TOATHREED and LINTOA are for tapes with time-of-arrival data. AOATHREED

and LINAOA are for tapes with angle-of-arrival data. AOACOR, along with CORWRITE and CORREAD, are for obtaining cross-correlograms for angle-of-arrival data only.

Plots for certain days showed unusual features and led to the making of separate plots for each of the scans, belonging to the area of interest. This led us to make standard (2-dimensional) plots. Again, 3 different sets of programs were made: time-of-arrival; angle-of-arrival; and correlograms, respectively. "Single scan" plots were also produced.

Using the same system for filenames as before, we created 3 programs:

- AOASCAN - for angle-of-arrival data.
- TOASCAN - for time-of-arrival data.
- AOACORSCAN - for correlograms.

All programs are written in FORTRAN extended version 4. for the CDC 6600 computer. All plots were made on the CALCOMP off-line pen plotter. During the debugging process, the TEKTRONIX display terminal and its hard copy machine were used to check the pictures.

APPENDIX A

#1	Blue card	<div>For "single scan" programs:</div> <div>CM = 150K (not including correlation)</div> <div>For 3-D programs:</div> <div>CM = 230K for angle-of-arrival tapes</div> <div>CM = 250K for time-of-arrival tapes</div>
#2	ATTACH,XX,{program name} ID=...,MR=1	Main program and subroutines (See list of program's names)
#3	FTN, ...	Compilation
#4	VSN(TAPE1 = {tape number})	Tape with <u>data</u>
#5	REQUEST, TAPE1, [:],L, NORING, NR. ({tape numbers})	[:] = $\begin{cases} \text{HI for angle-of-arrival tapes} \\ \text{HY for time-of-arrival tapes} \end{cases}$
#6	REQUEST, TAPE78,*Q.	Only for EEPLLOT plotter.
#7	DISPOSE, TAPE78,*HR.	Only for EEPLLOT plotter.
#10	ATTACH,X,THREED- 2WAY,ID=WIK,MR=1.	Can be excluded for "single scan" program, but then #13 has to be changed, i.e. not contain X.
#11	ATTACH,PEN,EEPLLOT. or ATTACH,TEK,TEKOFFLINE.	For EEPLLOT plotter For TEKTRONIX display

#12	REQUEST,T40140,*PF.	For TEKTRONIX only
#12 ^a	ATTACH,AAA,POTLIB.	Only for "single scan" plotting See #13 also.
#13	LDSET(LIB=X/TEK) LDSET(LIB=X/PEN) LDSET(LIB=X/TEK/AAA) LDSET(LIB=X/PEN/AAA)	} For "3-D" plotting } For "single scan" plotting
#15	LDSET(PRESET=ZERO)	
#16	LGO.	
#16 ^a	CATALOG,T40140, SCANPLOT,ID= ...	For TEKTRONIX only
#17	7/8/9	

17 ^a	1 or 0	ISWITCH (see main program) 1 - to make transformation of data 0 - to use data as is for plotting
#17 ^b	1 or 0	ISW6465 (see main program) 1 - for "early" tapes 0 - for regular tapes

Both 17^a and 17^b for angle-of-arrival tapes ONLY

- #18 NEW -1 Actually we don't use this card,
we only read it.
- #19 ☐ - any integer number
not 0 IISTEP. See main program
If we want to plot each scan, IISTEP=1
If we want to plot first scan, then skip
some of them, then plot again, we use
this parameter.
- #20 Example:
256 18 00 256 18 05 Start time - end time card
or
12 00
In this form it means : we want to start
from the beginning of the tape and plot
during 12 hours, or until end-of-file
mark.
- #21 1 86 060. Actually we don't use this card, we only
read it, for "single scan" program we
don't use it at all.
- #22 6 6. Actual and nominal spacing of data
signals. (each 6 seconds we received
next signal.)
- #23 10. 15. Length of X-axis for 3-D plotting.
Usually 10. for time-of-arrival and
correlation routines,
5. - for angle-of-arrival routines.
15. - angle of tilt for x-axis
For "single scan" plotting we don't
use, only read it.
- #24 Angle of arrival Label card
13 Sept. 1982
- #25 0 Number of gaps in data.

Example:

. #25^a 256 17 42 51

Special "time of the beginning" for
time-of-arrival tapes ONLY. To know
this time, we read it from corresponding
angle-of-arrival tape

#26 6/7/8/9-
green card

#3^a ATTACH, TAPE2,
SIGNAL, ID=...,
MR=1.

Only for run program CORREAD. File
SIGNAL has to be created before. We
created file SIGNAL during the execu-
tion of the program CORWRITE. See below

#5^a REQUEST, TAPE2,*PF.

Only for run program CORWRITE

#16^b CATALOG, TAPE2,
SIGNAL, ID=

Only for run program CORWRITE.

Tape CC0340 contains all programs:

AOATREED

TOATHREED

LINAOA

LINTOA

AOACOR

TOASCAN

AOASCAN

AOACORSCAN

CORWRITE

CORREAD

AOATHREED

TOATHREED = TESTLOS

LINAOA

LINTOA

AOACOR

AOASCAN

TOASCAN

AOACOR SCAN

CORWRITE

CORREAD

Tape

CC0340,

contains all programs.

REFERENCES

1. D. Nelson, Perspective Plotting of Two-Dimensional Arrays: Computer Program for a Digital Plotter, Maryland State University, College Park, Maryland, USA, 1966.
2. System/360 Scientific Subroutine Package, IBM, USA, 1970.
3. J. Bendat, A. Piersol. Random data: Analysis and Measurement Procedures., Wiley-Interscience, a Division of John Wiley & Sons, Inc., USA, 1971.



MISSION of Rome Air Development Center

RADC plans and executes research, development, test and selected acquisition programs in support of Command, Control Communications and Intelligence (C³I) activities. Technical and engineering support within areas of technical competence is provided to ESD Program Offices (POs) and other ESD elements. The principal technical mission areas are communications, electromagnetic guidance and control, surveillance of ground and aerospace objects, intelligence data collection and handling, information system technology, ionospheric propagation, solid state sciences, microwave physics and electronic reliability, maintainability and compatibility.

END

FILMED

7 - 84

DTIC